MAINLINE

MAINtenance, renewal and Improvement of rail transport iNfrastructure to reduce Economic and environmental impacts

Collaborative project (Small or medium-scale focused research project)

Theme SST.2011.5.2-6.: Cost-effective improvement of rail transport infrastructure

Deliverable 2.3:
Time-variant Performance Profiles for Life-Cycle Cost and Life-Cycle Analysis

Grant Agreement number: 285121 SST.2011.5.2-6.

Start date of project: 1 October 2011 Duration: 36 months

Lead beneficiary of this deliverable: SURREY

Due date of deliverable: 30/06/2013 Actual submission date: 03/12/2013

Release: Final

Project co-funded by the European Commission within the 7th Framework Programme		
Dissemination Level		
PU	Public	X
PP	Restricted to other programme participants (including the Commission Services)	
RE	Restricted to a group specified by the consortium (including the Commission Services)	
CO	Confidential, only for members of the consortium (including the Commission Services)	

Abstract of the MAINLINE Project

Growth in demand for rail transportation across Europe is predicted to continue. Much of this growth will have to be accommodated on existing lines that contain old infrastructure. This demand will increase both the rate of deterioration of these elderly assets and the need for shorter line closures for maintenance or renewal interventions. The impact of these interventions must be minimized and will also need to take into account the need for lower economic and environmental impacts. New interventions will need to be developed along with additional tools to inform decision makers about the economic and environmental consequences of different intervention options being considered.

MAINLINE proposes to address all these issues through a series of linked work packages that will target at least €300m per year savings across Europe with a reduced environmental footprint in terms of embodied carbon and other environmental benefits. It will:

- Apply new technologies to extend the life of elderly infrastructure
- Improve degradation and structural models to develop more realistic life cycle cost and safety models
- Investigate new construction methods for the replacement of obsolete infrastructure
- Investigate monitoring techniques to complement or replace existing examination techniques
- Develop management tools to assess whole life environmental and economic impact.

The consortium includes leading railways, contractors, consultants and researchers from across Europe, including from both Eastern Europe and the emerging economies. Partners also bring experience on approaches used in other industry sectors which have relevance to the rail sector. Project benefits will come from keeping existing infrastructure in service through the application of technologies and interventions based on life cycle considerations. Although MAINLINE will focus on certain asset types, the management tools developed will be applicable across a broader asset base.

Partners in the MAINLINE Project

UIC, FR; Network Rail Infrastructure Limited, UK; COWI, DK; SKM, UK; University of Surrey, UK; TWI, UK; University of Minho, PT; Luleå tekniska universitet, SE; Deutsche Bahn, DE; MÁV Magyar Államvasutak Zrt, HU; Universitat Politècnica de Catalunya, ES; Graz University of Technology, AT; TCDD, TR; Damill AB, SE; COMSA EMTE, ES; Trafikverket, SE; SETRA, FR; ARTTIC, FR; Skanska a.s., CZ.

WP2 in the MAINLINE project

The main objectives for WP2 are:

- To identify and model important degradation phenomena and processes for selected railway assets for the purpose of LCC and LCA
- To quantify the influence of intervention strategies on degradation time profiles
- To develop performance time profiles for selected asset types
- To validate the developed degradation and performance profiles through case studies.

Table of Contents

List of figures

List of tables

Glossary

Abbreviation/ acronym	**Description**
LCA	Life Cycle Analysis
LCAT	Life Cycle Assessment Tool
LCC	Life-Cycle Cost
NR	Network Rail
SKMA	SKM assessment
SQL	Structured Query Language (A data processing platform)
SRV	Slope Risk Value
SSHI	Soil Slope Hazard Index
w/c ratio	water cement ratio
WP	Work package

1. Executive Summary

The consensus from current railway asset management practice is that available deterioration models have been based on limited and scarce real data and/or that assumptions and idealisations have sometimes been transferred from other industry sectors without full validation. The MAINLINE project aims to improve available degradation and structural models in order to develop more realistic life cost and safety estimates for asset management purposes. As part of this effort, the present work focuses on the development of performance-time profiles for a diverse group of railway assets, namely track, soil cuttings, metallic bridges and concrete lined tunnels. The methodologies for developing performance-time profiles based on different criteria related to the condition or the capacity (resistance) of the asset are presented. For each asset type, a wide range of environmental and service conditions is considered, in order to cover different possible scenarios relevant to the European railway infrastructure. Example profiles are given for each asset type investigated. The outputs from this work will be made available to the Life Cycle Assessment Tool developed by the MAINLINE consortium.

2. Acknowledgements

This present report has been prepared within Work Package WP2 of the MAINLINE project by the following team of contractors, with the University of Surrey acting as deliverable co-ordinator and work package leader:

- SETRA – concrete tunnels
- SKM – soil cuttings
- TU Graz – track
- University of Surrey – metallic bridges

Fruitful discussions with all MAINLINE partners are gratefully acknowledged.

Particular thanks are due to the members of the Project Advisory Committee who have undertaken the technical review of the present deliverable: Dr Rosemarie Helmerich (BAM) and Dr Livia Pardi (Autostrade).

3. Introduction

The present report constitutes Deliverable D2.3: Time-variant Performance Profiles for Life-Cycle Cost and Life-Cycle Analysis emanating from WP2: Degradation and structural models to develop realistic life cycle cost and safety models. Building on Deliverable 2.2: Degradation and Intervention Modelling Techniques[1], the present report focuses on the methodologies adopted for the development of time-variant performance profiles for selected asset categories. The assets selected follow directly from the work undertaken in D2.2 and are as follows:

- Track (plain line)
- Soil cuttings
- Tunnels with concrete lining
- Metallic bridges

In D2.2, masonry lined tunnels were also investigated in terms of their deterioration mechanisms but the development of performance profiles was not feasible due to the scarcity of analytical models coupled with the lack of field data. Thus, neither empirical nor analytical performance profiles would have been possible and it was decided, following consultation with Network Rail who is the main infrastructure owner of such assets, to exclude masonry lined tunnels from further analysis.

As mentioned in Deliverable 2.2, in moving from degradation to performance profiles, it is important to distinguish between condition-governed and capacity-governed asset profiles. The assets analysed herein are characterised by both profile types, with the latter (capacity-governed) being particularly relevant to the life-cycle analysis of bridges and tunnels (structural assets), whereas the former (condition-governed) are relevant to track and soil cuttings.

The results presented in this report feed into Task 5.5: Development of MAINLINE LCAT. Figure 3.1 shows schematically the general organisation of the project into work packages (WPs) and identifies the main interactions. WP2 interacts with WP1, WP4 and WP5. The interaction with WP1 consists of inputs for degradation and performance models that will be developed within WP1 and will also be utilised within WP2. The two-way interaction with WP4 is focused on identifying model parameters for the degradation and structural models that would benefit (in terms of the confidence with which they can be specified in models) through monitoring and examination. As mentioned above, the main outputs from WP2 in terms of time-dependent performance profiles will be passed on to WP5.

[1] MAINLINE Deliverable 2.2 is available on line from: http://www.mainline-project.eu/Results,7.html

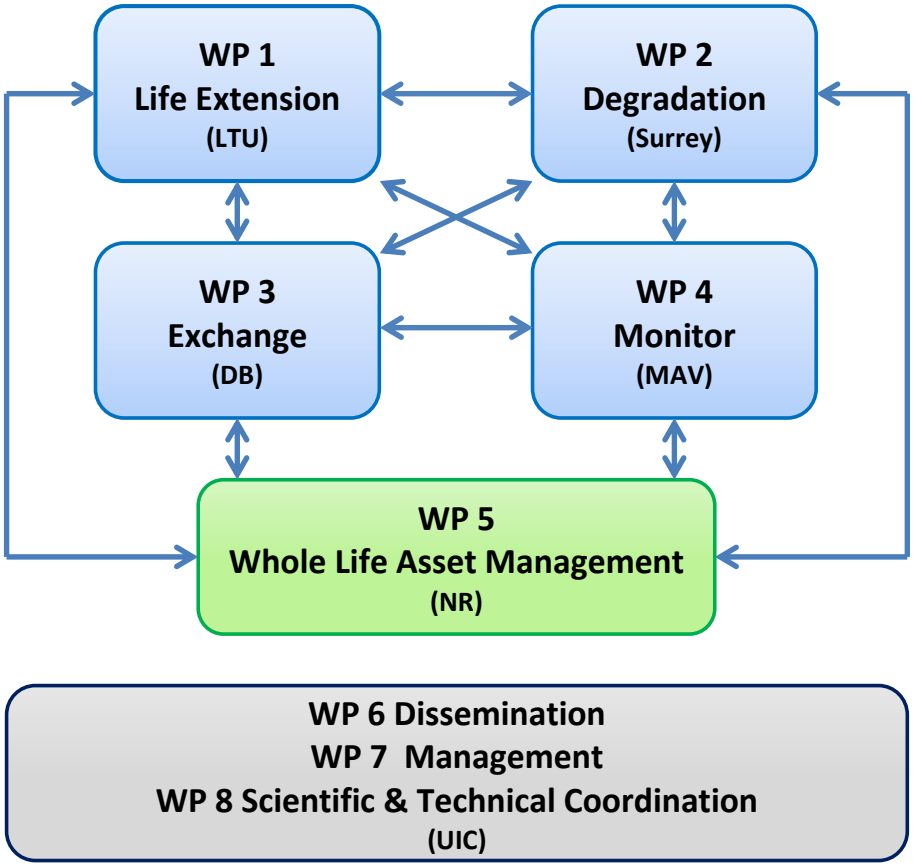

Figure 3-1 General organisation of the project

Part n°	WP2 Partners	Country
1	UNION INTERNATIONALE DES CHEMINS DE FER - UIC	FR
2	NETWORK RAIL INFRASTRUCTURE LTD	UK
3	COWI A/S	DK
4	SINCLAIR KNIGHT MERZ	UK
5	UNIVERSITY OF SURREY	UK
6	TWI LIMITED	UK
10	MAV MAGYAR ALLAMVASUTAK ZARTKORUEN MUKODO RT	HU
12	TECHNISCHE UNIVERSITAET GRAZ	AT
17	SERVICE D'ETUDES SUR LES TRANSPORTS, LES ROUTES ET LEURS AMENAGEMENTS	FR

4. Track

4.1 Context

The main parameter influencing the deterioration processes of track, the necessary maintenance actions following the deterioration and the track service life, generally, have been described in Deliverable 2.2. Most relevant for decision making, in terms of allocating funding for maintenance (or alternatively for track renewal) are the actual maintenance cycles. Whether or not these cycles indicate the need for a renewal depends on the component analysed:

- Rail wear/fatigue/damage: In general these deterioration processes are not critical for the overall service life of track. Rails can be changed quite easily if further maintenance is no longer possible due to reached geometrical limits, even though this is a costly measure.
- Rail fastenings: As long as the sleepers do not show significant damage, it is possible to change or re-fasten the rail fasteners.
- Sleepers: In the case of concrete (or steel) sleepers, the service life of the sleepers should be long enough not to limit the track service life – always assuming that maintenance is properly executed. Wooden sleepers can – under certain circumstances – be the limiting component for the total track.
- Ballast: Worn ballast results in several consequences. Track geometry has to be corrected more frequently when ballast loses its original quality; reduced tamping intervals with advancing track service life are the maintenance response. The fine material originating from the deterioration processes (edge breaking, abrasive wear) trickles through the ballast bed and accumulates at the bottom. This rising percentage of fine material leads to a stiffer ballast bed which reduces the elasticity of the system track. This is crucial for the other components as reduced load distribution leads to increased stresses due to load concentration. Ballast cleaning can re-establish a proper grain-size distribution, but it is a very expensive process leading to massively increased life cycle costs. Therefore, ballast is, in most cases, the critical component which dictates the economic renewal of track.
- Subsoil & drainage: even though both these features have a high impact on the possible service life, either maintenance can be done quite easily (e.g. cleaning ditches) or improvements will only be feasible during general renewals.

In view of the above factors, the ballast is the best indicator for service life of track and the on-site tamping cycle is a proper sign for life time estimation.

4.2 Development of performance function

Extensive data analyses, as highlighted in D2.2, lead to the following conclusions:

- Tamping demand is described by the track riding quality.
- The intervention level has massive influence on the achievable quality following maintenance.
- There is a strict relation between tamping cycle and service life.

A model estimating track service life must, therefore, be based on the track quality behaviour considering tamping actions derived from track riding quality. Additionally, the status of other

components must be checked in order to guarantee the estimated service life. Maintenance has a major impact on the outcome, as insufficient or wrong maintenance can lead to a reduced service life.

Building on research results from over ten years, the track quality index deteriorates on the basis of the following exponential function:

$$Q_{(t)} = Q_n \times e^{b \times t} \qquad (4.1)$$

Starting point is the initial quality (Q_0) at track relaying – or the quality level Q_n after tamping. This quality level is artificial as it is extrapolated back to the starting point in time with a regression function using the measured or calculated quality against time. Therefore Q_n signifies the initial quality including initial settlements. The exponent b (deterioration rate) indicates the speed of the deterioration process over time (t) under different impacts.

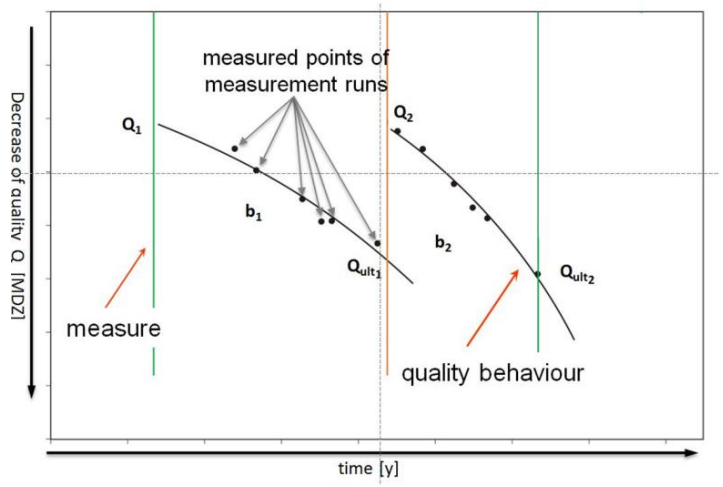

Figure 4-1 Time profiles for the track quality index

The deterioration rate is influenced by the following factors:

- Track alignment
- Subsoil condition
- Ballast quality
- Draining functionality
- Superstructure components
- Transport load

The transport load is a rough indicator of a number of influences including type of vehicles in use, speed and total loading. Furthermore the deterioration is influenced by the maintenance executed and the quality of the executed work, which affect the quality regained by the maintenance. This last point has to be particularly highlighted: Seen from the track quality point of view, the boundary conditions as well as the maintenance lead to higher or lower deterioration rate – in the end it is only the quality function that determines the further needs for interventions.

To enable a prognosis of future behaviour and maintenance needs, it is essential to describe the parameter as well as possible. While it might be comparatively easy to describe the superstructure (e.g. 60E1 rail with a R260 steel grade on concrete sleepers with under sleeper pads), or to collect the transport load as the yearly sum of gross ton kilometres, there is hitherto no way to define the condition of the subsoil and the drainage system by a single value or a set of values.

Moreover it is unlikely that all future users of the LCAT will have all the necessary data available to define the detailed deterioration process. Two scenarios are possible: In one case, basic information on the track status is available (type of superstructure, age, transport load, subsoil categorisation). This information can be used for a rough estimation of the deterioration process that has to be specified by additional information of the user in a second step. In the other case, the track age and the tamping cycle are available, allowing the same procedure as described before.

traffic loading		<15.000 [t/d]		
		15.000 - 30.000 [t/d]		
		30.000 - 45.000 [t/d]		
	x	45.000 - 65.000 [t/d]		
		> 65.000 [t/d]		
track age		[a]		
operating speed	130	[km/h]		
ballast		hard	[basalt, hq granite, siliceous material]	LA<16
	x	medium	[granite,diabase, dolomite]	LA<23
		soft	[limestone]	LA>23
sleeper	x	concrete		
		concrete with under sleeper pads		
		wooden		
radii		<250m		
		250m - 400m		
		400 - 600m		
	x	>600m		
sublayer condition	x	good		
		bad		
drainage condition	x	good		
		bad		
avg. tamping cycle	3	[a]		

Figure 4-2 Template for categorisation of track deterioration profiles

In order to establish such an approach, several “templates” (i.e. typical categories leading to deterioration profiles) are provided as starting points for an interpolation. These profiles are set up for different transport loads, different types of sleepers and different track alignments. These profiles are accompanied by a check list, which the LCAT user will have to go through, answering questions on component details (ballast type, status of sleepers, etc.), a subsoil categorisation, and some important measured values (e.g. stability of the gauge signal). The prognosis of future maintenance demands and the service life is then carried out using general research results, like “bad subsoil condition” leads to % increase of tamping demand and % less service life. Deterioration profile templates start with the minimum information, as depicted in Figure 4-2.

This parameter-set was analysed using a databank of measured quality data, executed maintenance, and track status data over a period of ten years. The quality data measured along the track was stored and re-positioned run by run. Within the analysis the x-axis turns from “track km” to “time” for a discrete point of track, see Figure 4-3.

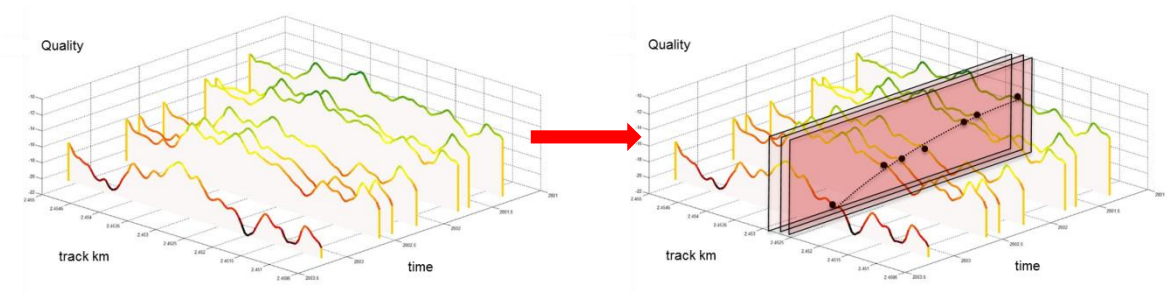

Figure 4-3 Schematic generation of track quality profiles

Following this transformation, the deterioration function can be visualised and the corresponding values of Q_n and b can be calculated, see Figure 4.4.

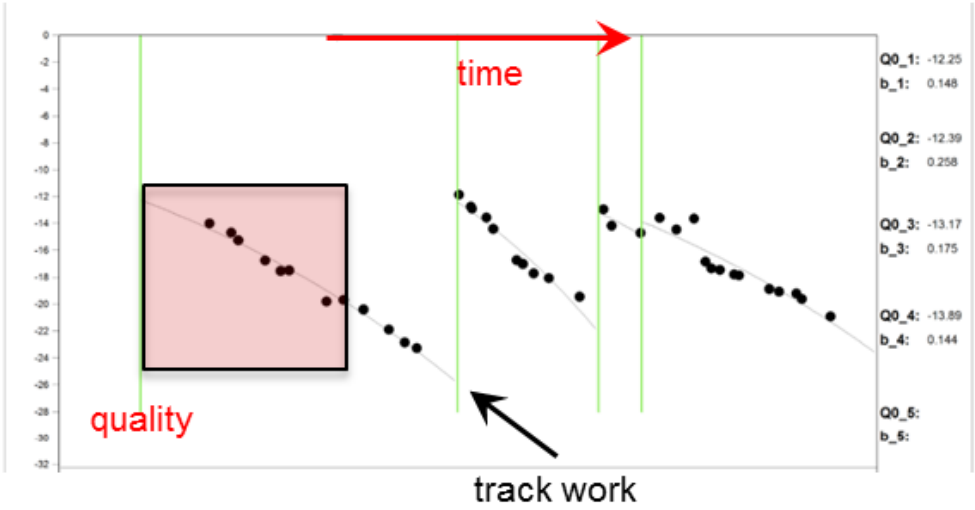

Figure 4-4 Parameter estimation for track quality profiles

Following this approach, track with the same parameters can be identified and analysed network-wide, resulting in a large number of quality levels and b-rates. The mean values of these two values are used to set up a generally valid deterioration profile. As described in deliverable D2.2, the intervention level has a high impact of the whole life deterioration process: Higher intervention levels for newly laid track guarantee high quality levels, while reducing requirements as end of life approaches, and help to squeeze out additional service life.

In addition to intervention levels, deterioration rates also change over the service life: Generally it can be stated that the quality level decreases over time, while the deterioration rate (b) increases. For the parameter sets including concrete sleepers, it must be considered that the initial settlements after relaying are quite high. After some years the track stabilises, behaves quite well for some time and then starts deteriorating faster at the end of service life. By way of example, Figure 4-5 shows the overall evaluation of deterioration rates and quality levels for different track ages.

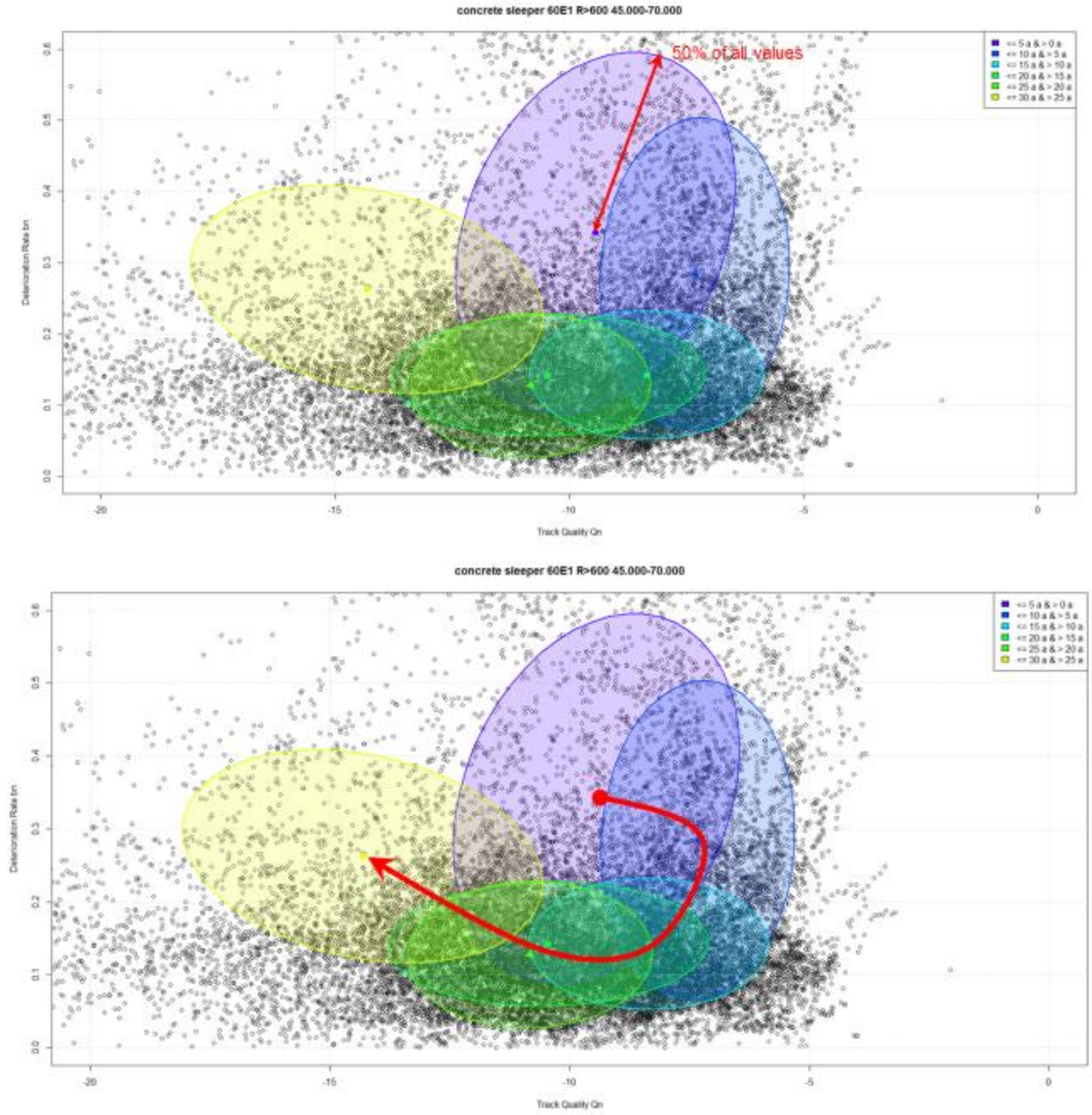

Figure 4-5 Scattergrams of deterioration rate values for different track conditions

Track quality runs through the described deterioration process (red curve), intercepted by several tamping actions whenever the intervention levels are reached. The resulting work load is shown in the next graph. Seen from the technical point of view, tamping actions could be executed very intensively at the end of the service life. If quality starts to be very instable, tamping is often not enough to guarantee a safe operation – speed restrictions are a consequence of this. While technical behaviour can be described quite well using this deterioration model, the follow-up economic evaluation has to establish, at which point in time, the rising maintenance and operational costs exceed the reduced depreciation costs.

Within the MAINLINE project it is proposed to evaluate such deterioration processes for **three** types of sleepers, **two** transport loads and **two** different alignments. As subsoil condition for example is set to “sufficient”, weak subsoil conditions are not covered by the templates.

From the overall evaluations, general rules are formulated to interpolate and extrapolate from these discrete parameter sets to different values. By way of example, Figure 4-6 gives an idea of the impact of inadequate subsoil or drainage not working properly. Both the deterioration rate and quality level show significantly worse levels compared to the “good subsoil” scenario. For the main parameter transport load and alignment similar evaluations are carried out in order to support the LCAT user as well as possible.

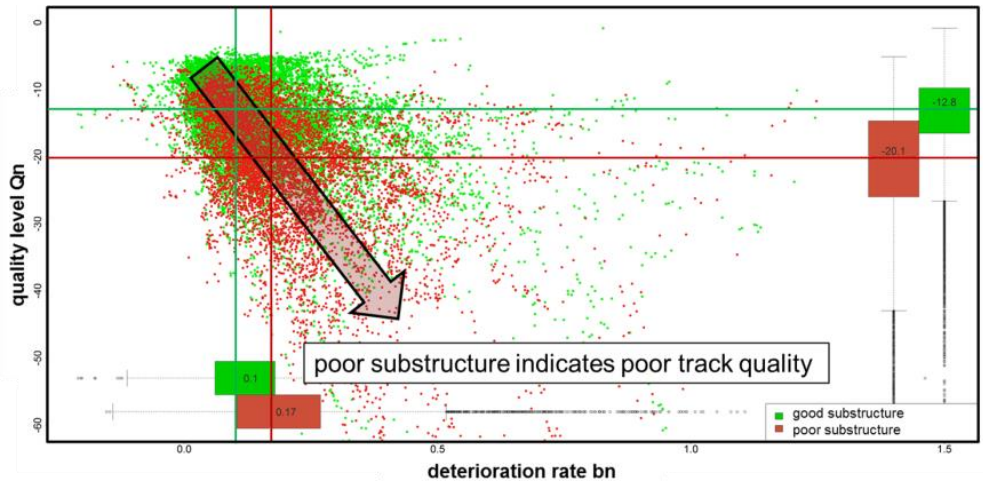

Figure 4-6 Example of discriminant analysis

It must be emphasized that the service life estimated through this deterioration process can be shortened in the economic evaluation by the maintenance demands of other track components. Rail exchange at the very end of the service life could lead to rising costs limiting the potential service life of the ballast bed. The same holds in the case of massive deterioration of sleepers, especially wooden sleepers, as sleeper exchange can also lead to higher life cycle cost. From track life cycle monitoring experience, the following maintenance demands are generally critical for the service life of track:

- Tamping cycles shorter than one year
- (Partly) Sleeper exchange
- Rail exchange at the end of service life
- Ballast cleaning at the end of service life
- Permanent speed restrictions in general

The deterioration profiles worked out for the LCAT in WP 5 for track therefore characterise a potential service life that has to be specified due to additional information.

5. Soil Cuttings

5.1 Context

This section shows how the deterioration profiles were derived from the soil cuttings data described in document D2.2.

5.2 Source data

As described in D2.2, historical data, from Network Rail (NR) in the UK, were used to derive the deterioration profiles. This is the only known source of extensive, numerical, historical data from which trends can be derived. The NR soil cutting scoring system is known as the Soil Slope Hazard Index (SSHI) and the data includes details of the location and date of each examination but crucially describes the critical features and condition of the soil slopes in terms of predefined characteristics with alpha-numeric scores.

5.2.1 Scoring systems

In order to make the condition criteria more usable by other infrastructure managers the scoring system has been simplified from SSHI for use in the LCAT. The revised scoring system derived by SKM is known in the context of this project as the SKM Assessment (SKMA). The conversion process is described in the D2.2 report.

The key scores for the cuttings in the SKMA systems can be divided into two parts: those which are assumed to be essentially permanent over the life of the LCAT model (e.g. soil type and overall geometry) and those features which may vary (e.g. drainage and vegetation). The full list of variables is given below:

Group	Score	Characteristic measured
Permanent	ST	Soil Type: Granular, Cohesive or Inter-bedded
	SHF	Slope Height Factor: height and angle
	ALF	Adjacent Land Factor: slope and drainage of adjacent land
Variable	MA	Movement Assessment: heave or bulge on slope or toe
	VA	Vegetation Assessment: extent of trees and grass
	SW	Surface Water Assessment: extent of surface water
	DA	Drainage Assessment: condition of drains, if any
	BA	Burrowing Assessment: extent of animal burrowing
	CA	Construction Activity Assessment: presence of construction work

The scores assigned to each variable are based on the presence of various features in the cutting as specified by the SKMA. For a given variable, scores are provided for the various possible combinations of features, with the worst (highest) score being assigned when there is more than one combination present.

These scores were combined to give an overall Slope Risk Value (SRV) which typically varied between 0 and 20, the higher values indicating more risk.

The LCAT model is designed to forecast the likely condition of the cutting and, because of the complex relationships between the six variables listed above, it was decided to model the deterioration of each variable separately. The three 'permanent' scores are assumed to remain constant. It was therefore necessary to establish the likely changes in these six variables over time. This was achieved by estimating the mean change in each variable after 5-years, based on the historical records made available by NR.

The process of deriving these expected values is described below.

5.3 Processing of historical data

The Soil Slope Hazard Index (SSHI) data collected by Network Rail is currently the only expansive and sufficiently detailed set of condition data for cuttings available to the MAINLINE project. Within Network Rail's cuttings SSHI algorithm there are thirty "Stability Index Parameters", each measuring a separate characteristic of slope in question. These Stability Index Parameters include such characteristics as Slope Angle and Slope Height, Geological Strata and so on.

Each Stability Index Parameter features a number of sub-options called "Observed / Measured Values", hereafter referred to as Observed Values. Each Observed Value either features or does not feature for a particular slope, and when undertaking a condition examination for a slope the presence or absence of every Observed Value is assessed as across all Stability Index Parameters. For some Stability Index Parameters the Observed Values are exclusive (e.g. Slope Height, where the options are <3 m; 3-10 m; >10 m) and for others the Observed Values are cumulative (e.g. slope face drainage conditions, where any of the following options can be present in any combination: Face dry / Functioning drainage / Blocked drainage / Marshy areas on slope / Surface issues on lower slope / Surface issues on upper slope).

NR was able to provide 124,709 numerical records of examinations of 68,555 sections cutting slopes, each approximately 100-metre (5-chain) section of the side of a cutting being a separate slope record. The records extended over the period from March 2000 to February 2012. Some sections had only been inspected once and some as many as 14 times. The data was processed to establish 14,556 sections which had been inspected more than once and had readings which could be converted into the six SKMA variables mentioned above. The records for these sections formed the basis of the deterioration analysis.

5.3.1 The SSHI Algorithm

The SSHI algorithm contains weighted scores for each Observed Value in terms of the level of risk they are thought to contribute to each of the five defined failure modes (Rotational, Translational, Earthflow, Washout and Burrowing).

These collected Observed Value scores are processed in a particular way to obtain a single high level risk score for the slope; the slope's Soil Slope Hazard Index (SSHI) – a number that due to the idiosyncrasies of the algorithm sits between 2 and 16.

This number is used to assign an overall condition classification to the slope (Serviceable, Marginal, Poor or Top Poor), which is a key input into the basis of Network Rail's approach for managing the asset; driving for example choice of remedial solution (if any), frequency of examinations and more.

More information on the format and function of the SSHI algorithm is available from the following Network Rail Documents:

- Earth structures Algorithm Methodology Rev 4.doc
- SSHI algorithm new soil weightings rev 8.1 (Final) - SET.xls

5.3.2 The MAINLINE condition scoring system for cuttings – SKMA

The SKMA condition scoring system for cuttings developed for MAINLINE operates on a very similar basis as Network Rail's SSHI algorithm; a series of detailed observations regarding individual, defined characteristics are converted into numeric values and combined according to rules to give an overall number indicative of the risk of the slope.

The SKMA algorithm, which has been explained in full detail in D2.2, has been specifically designed taking into account a number of principles, including the following:

- Its inputs should be less detailed than those required for the SSHI algorithm, since it is otherwise unlikely that any infrastructure operators other than Network Rail will have the data available to populate it
- Its inputs should be a subset of those required for SSHI (or as closely match this as possible), so that it becomes possible to generate a SKMA score from a set of SSHI Observed Value data without the need for further examination of the asset in the field.

The second bullet point effectively means that the primary Observed Value data collected by Network Rail for their SSHI algorithm (i.e. whether each Observed Value characteristic is present or not) can be "translated" (mapped) into SKMA algorithm inputs, which can then be used to generate a SKMA score in a similar way as the SSHI inputs are used to calculate an SSHI score. This translation process effectively allows the MAINLINE project to use Network Rail's eight years of SSHI examination data as the basis for an analysis of the deterioration of cuttings assets over time expressed in terms of SKMA scores.

The observations made during each SSHI examination are recorded via a series of alphanumeric codes which identify certain features present in the cutting. For example, codes A1 through to A12 are used to describe slope angle and height, with A4 say indicating a slope of angle greater than 35 degrees and height less than 3 metres. These alphanumeric codes were analysed and grouped into sets corresponding to the six variables described above. It was then possible to map the SSHI features to the SKMA features, and then an overall SRV value could be assigned. The following sections describe the process of mapping Network Rail's SSHI data to the MAINLINE project's SKMA inputs for this purpose.

5.3.3 SSHI to SKMA conversion process

The scores were converted from the SSHI system to the revised SKMA system. Rather than map the SSHI scores directly to the SKMA scores, the SSHI *features* were mapped to the SKMA *features* and then appropriate scores in the SKMA system were assigned to each feature.

Each input required for SKMA is assessed individually. The available fields in SSHI (each Stability Index Parameter and, within these, all Observed Values) are assessed for their relevance to the SKMA input in question, and where an Observed Value is deemed to be significant its possible values are mapped to the SKMA inputs accordingly.

An example mapping is as follows; for Adjacent Land Slope, which is informed by the field "Slope angle adjacent to earthwork" in SSHI:

SKMA	
Adjacent Land Slope	
ALF1	-'ve slope
ALF2	No slope
ALF3	+'ve slope

SSHI	
Slope_Angle_Adjacent	
1	(-)ve falls away from earthwork
2	(+)ve falls towards e/work <5 degrees
3	(+)ve falls towards e/work 5 to 15 degs
4	(+)ve falls towards e/work >15 degs

SSHI > SKMA Conversion Assumptions		
Slope_Angle_Adjacent		SKMA_ALF_Slope
1	(-)ve falls away from earthwork	ALF1
2	(+)ve falls towards e/work <5 degrees	ALF2
3	(+)ve falls towards e/work 5 to 15 degs	ALF3
4	(+)ve falls towards e/work >15 degs	ALF3

The process is made complex by the structure of the SSHI data, but essentially it is this simple mapping methodology by which all SKMA inputs are identified from the SSHI inputs. The following features of the SSHI data in particular make the mapping complex:

1) Each Stability Index Parameter field within the SSHI data can feature multiple Observed Values; all concatenated one after another in a large text string.
2) Multiple Stability Index Parameter fields may need to be referenced for a single SKMA input.
3) Movement Indicator records are stored in a many-to-one relationship vs. examination records within the SSHI data.
4) Repeat exams are not easily identifiable within the SSHI data; start and end mileages are seen to vary (to a range of extents) across different exams.
5) All Observed Values are returned in the SSHI data; so processing logic is required to assess the two worst-scoring characteristics according to the SKMA methodology in order that they can be selected and applied.

Nonetheless assumptions and processing steps can be put in place to overcome these.

The entire conversion process is conducted in an SQL 2005 database via a series of 43 queries which reference the eight years of Network Rail SSHI data; identifying repeat examinations and transforming their characteristics into SKMA scores.

5.3.4 Conversion Tables

The high level mapping of inputs from SSHI to SKMA are as follows:

SKMA		SSHI	
Element	**Description**	**Field Description**	**Field Code**
ALF	Adjacent Land Slope	Slope angle adjacent to earthwork	B
	Adjacent Land Features	Drainage of adjacent land	K
		Geomorphology of Adjacent Land	V
SHF	Slope Height	Slope Angle and Slope Height	A
	Slope Angle	Slope Angle and Slope Height	A
CA	Construction Activity 1	Construction activity at slope crest	D
	Construction Activity 2	Construction activity at slope crest	D

SKMA		SSHI	
Element	**Description**	**Field Description**	**Field Code**
BA	Burrows	Burrows	CC
DA	Drainage Feature 1	Slope face drainage conditions	J
		Slope crest drainage	Q
		Cess Drainage	T
	Drainage Feature 2	Slope face drainage conditions	J
		Slope crest drainage	Q
		Cess Drainage	T
SW	Surface Water Feature 1	Slope face drainage conditions	J
		Slope erosion	S
		Mass movements	Z
	Surface Water Feature 2	Slope face drainage conditions	J
		Slope erosion	S
		Mass movements	Z
VA	Vegetation Feature 1	Cracking	Y
		Tree Cover	DD
		Ground Cover	EE
	Vegetation Feature 2	Cracking	Y
		Tree Cover	DD
		Ground Cover	EE
MA	Movement Feature 1	Slope form of Earthwork	U
		Track Movements (vis. to naked eye)	W
		Mass movements	Z
	Movement Feature 2	Slope form of Earthwork	U
		Track Movements (vis. to naked eye)	W
		Mass movements	Z

The detailed field transformations within these linkages have not been described here (the information is too extensive) but these have been tabulated and are available from the MAINLINE project team if required. Specific details of the conversion steps are given in Appendix A to this report.

5.4 Collating the SKMA deterioration

The soil type of each slope was classified as granular, cohesive or inter-bedded. In some cases the same slope was recorded as a different soil type in different examinations; in these cases the soil type was assumed to be inter-bedded. This classification resulted in 11,023 sections of inter-bedded slope, 2,131 granular and 1,402 cohesive.

The paired examinations were typically separated by a time interval of between about one and five years. The change in scores over this interval in each case was then linearly extrapolated to the change in 5 years. This data was classified by the initial score from which is started, so that typically for each possible initial score value a number of projected scores after five years were established.

It was noted that those slopes assumed to be in ‘poor’ condition had generally been inspected more frequently, typically annually, whereas the ‘serviceable’ slopes were

inspected only every five years. This is understood to be in accordance with Network Rail's Risk based Examination processes (standards) for their earthwork asset examinations. The resulting high incidence of readings for 'poor' slopes tended to skew the data. It was therefore decided to average the changes in score for each slope before averaging these results across all the slopes. This process ensures that the data from all slopes receives the same weighting despite the more frequent examinations of the 'poor' slopes.

The resulting dataset gave the mean change in score, classified by:

soil type (3 possible types)

score variable (6)

starting score (2 to 7 depending on variable)

It should be noted that the behaviour is not differentiated by the slope height or angle but this is considered valid within the scope of the SKMA risk evaluation system.

In one case, a gap was found where a particular initial score (Granular, Vegetation Assessment with initial score 0.5) was not represented in the data. The rate of change in this case was taken as the mean of the changes to the adjacent values of the same variable.

The resulting tables of deterioration are included in Appendix B to this report. The NR SSHI data was processed into the deterioration tables using a SQL server database and Excel spreadsheets. The summary data is a small set of tables which can be transferred to the LCAT model in Excel.

5.5 The influence of Interventions

The correlation of interventions and changes in condition scores has not been systematically recorded for soil cuttings. Consequently no definitive score changes can be attributed to interventions. However, major repairs to earthworks, for example, or to the drainage system will have the effect of resetting the relevant scores to their lowest values.

5.6 Conclusions for soil cuttings

The deterioration rates derived here are entirely based on historical data and include no theoretical forecasting of deterioration mechanisms.

Slope condition data from eight years of examinations by Network Rail (UK) has been processed to provide the likely change in six condition score over a five-year period. These deterioration rates are available for various configurations of slope, soil types and starting conditions. The scoring system used was adapted by NR's SSHI system to a more simplified system known as SKMA.

In sufficient data is currently available to allow the influence of interventions on condition scores to be reliably evaluated, but some reasonable assumptions can be made about the effect of major improvement works on particular scores.

6. Metallic Bridges

6.1 Introduction

This section presents the methodology for determining performance profiles of metallic railway bridges subject to deterioration due to corrosion. The objective is to combine coating and corrosion damage modelling, presented in D2.2, with structural analysis methods, in order to generate performance profiles for typical bridge elements, which can be included in the Mainline LCAT tool.

In previous studies dealing with performance assessment of corroding steel bridges (e.g. Kayser & Nowak 1989, Czarnecki & Nowak 2008, Sharifi & Paik 2011), a systematic exposure classification was lacking and corrosion damage was predicted from models based on non-homogeneous databases. Furthermore, in most studies the time-dependent performance of the protective system, which needs to be broken down before corrosion damage occurs, was not considered explicitly. The present work aims to overcome these limitations and develop a framework which can be applied for a variety of bridge environments, coating types and structural elements. Emphasis is given to the consistent exposure classification, and a distinction is made between condition and capacity based performance criteria. The methodology is demonstrated through a typical half-through steel bridge for which a family of performance profiles is developed. Further performance profiles are developed for a truss bridge to cover structures for which axial loads are dominant.

6.2 Modelling principles

6.2.1 Influencing factors & exposure classification

Coating deterioration and steel corrosion (following the loss of protection provided by the coating) are time-dependent processes, with their rate being determined by the exposure conditions experienced by the bridge. The possible types of outdoor exposure environments that may be experienced by a structure can be broadly classified under as: (a) immersed, (b) splash zone and (c) atmospheric exposure, see Figure 6-1. Each of these environments is associated with different ranges of corrosivity potential. This study focuses on the deterioration modelling of steel bridges affected by atmospheric corrosion. Atmospheric exposure can itself be subdivided in a number of categories based on their corrosivity harshness, represented as rural, urban and industrial/marine exposures.

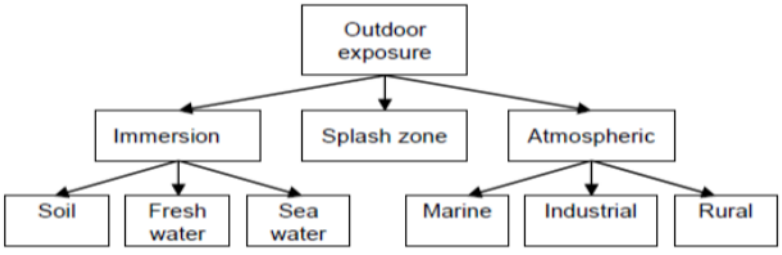

Figure 6-1 Outdoor exposure environments (Sorensen et al. 2009)

Several studies (e.g. Feliu et al. 1993, Klinesmith et al. 2007, EN ISO 2012:9223), unanimously concluded that the main parameters influencing the corrosivity of an atmosphere include climatic factors (i.e. relative humidity and temperature) and atmospheric pollutants (i.e. sulphur dioxide SO_2 and chlorides Cl^-). The physical monitoring of these parameters would enable the atmospheric corrosivity classification of a particular area. Furthermore, the correlation of these exposure parameters with metal loss measurements has allowed the development of corrosion models, as discussed later. The standard EN ISO 9223 (2012) provides a framework for the classification of atmospheric corrosivity based on the levels of the main influencing climatic and pollutant parameters. More specifically, in EN ISO 9223 (2012), the spectrum of atmospheric corrosivity is divided in five categories varying from very low corrosivity (category C1), corresponding to rural environments, up to very high corrosivity (C5) and extreme corrosivity (CX). Table 6-1 provides a brief description of each corrosivity category together with the expected ranges of corrosion rates within each category.

Table 6-1 Description of outdoor atmospheric corrosivity categories and corresponding corrosion rates in EN ISO 9223 (2012)

Corrosivity category	Description	Corrosion rates [1] (μm/year)
C1	***Very low corrosivity***: Dry or cold zone, atmospheric environment with very low pollution and time of wetness, e.g. certain deserts, Central Arctic/Antarctica.	≤ 1.3
C2	***Low corrosivity***: Temperate zone, atmospheric environment with low pollution (SO_2 < 5 μg/m^3), e.g. rural areas, small towns. Dry or cold zone, atmospheric environment with short time of wetness, e.g. deserts, subarctic areas.	1.3 < *A* ≤ 25
C3	***Medium corrosivity***: Temperate zone, atmospheric environment with medium pollution (SO_2: 5 μg/m^2 to 30 μg/m^3) or some effect of chlorides, e.g. urban areas, coastal areas with low deposition of chlorides. Subtropical and tropical zone, atmosphere with low pollution.	25 < *A* ≤ 50
C4	***High corrosivity***: Temperate zone, atmospheric environment with high pollution (SO_2: 30 μg/m^3 to 90 μg/m^3) or substantial effect of chlorides, e.g. polluted urban areas, industrial areas, coastal areas without spray of salt water or, exposure to effect of de-icing salts. Subtropical and tropical zone, atmosphere with medium pollution.	50 < *A* ≤ 80
C5	***Very high corrosivity***: Temperate and subtropical zone, atmospheric environment with very high pollution (SO_2: 90 μg/m^3 to 250 μg/m^3) and/or significant effect of chlorides, e.g. industrial areas, coastal areas, sheltered positions on coastline.	80 < *A* ≤ 200
CX	***Extreme corrosivity***: Subtropical and tropical zone (very high time of wetness), atmospheric environment with high SO_2 pollution (higher than 250 μg/m^3) including accompanying and production factors and/or strong effect of chlorides, e.g. extreme industrial areas, coastal and offshore areas, occasional contact with salt spray.	200 < *A* ≤ 700

Notes: [1] Corrosion rates correspond to the first year of exposure (coefficient *A* in Equation 6.1).

In considering the deterioration of complex and spatially extended structural systems such as bridges, individual elements (e.g. deck, main girders, cross beams, etc.) are likely to experience dissimilar deterioration rates due to differences in the microclimate which develops in their immediate surroundings (Hutchins & McKenzie 1973). For instance, a Japanese survey showed that external main girders of steel-composite bridges are more susceptible to corrosion than inner girders (Tamakoshi et al. 2006).

In simple terms, corrosion can be classified as general or local, though a more precise classification based on the forms of corrosion can also be relevant (e.g. Landolfo et al. 2010): general (uniform), pitting (localised), crevice, erosion, galvanic and fatigue corrosion. It is important to point out that during different time stages, a localised form can spread spatially or, conversely, a uniform domain can develop localised patterns. The rate of deterioration due to atmospheric corrosion is determined by the levels of key climatic variables (temperature and relative humidity) and airborne pollutants (e.g. sulphur dioxide and chlorides), as well as the maintenance level and the properties of the protective system applied on the structure.

6.2.2 Types and performance of protective coatings

Several coating types – of varying composition and performance – exist for the protection of structural steelwork. The coating types used, and their durability characteristics, are described in Part 5 of EN ISO 12944 (1998). In general, their durability is classified as low, medium and high, with indicative times given as 2-5, 5-15 and more than 15 years. For the UK rail industry, current recommendations distinguish between new and existing steelwork and a number of coating systems are recommended for each (NR 2009a, b and c). Commonly used coatings for new construction include duplex systems in which the first of several layers is a metallic coating, for instance thermally sprayed zinc or aluminium. On the other hand, a number of coating systems for maintenance of existing structures also are available, broadly subdivided into those recommended for patch repairs (bitumen based) and those for complete re-application. These protective systems typically consist of several layers applied sequentially on the treated steel surface. The performance of a coating system is influenced by several factors, including, among others, the composition and exposure conditions, as well as workmanship and quality control during application. Table 6-2 summarizes the characteristics and expected service life of two coatings used in maintenance. Estimates for the expected service life of different coating systems currently used in the UK railway infrastructure are given in industry standards (NR 2009a, b and c).

Table 6-2 Description and expected service life of protective coatings (NR 2009a and b)

Coating system name	**Description** [for more details see (NR 2009a, b)]	**Expected life, L_T (years)**
M27.4	***Protective system using bitumen***. 1st layer: surface tolerant epoxy primer (min dft 100µm. Intermediate coat: gelled bituminous solution – aluminium tinted (min dft 200µm). Topcoat: gelled bituminous solution – black finish with min dft 200µm.	5-7
M21	***Coating using epoxy glass flake***. 1st layer: epoxy blast primer with min dft 25µm. Intermediate layer: epoxy glass flake intermediate coat with min dft 40µm and for layer C select among the following (min dft 50µm): anti-graffiti paint or polyurethane coloured finish or acrylic urethane topcoat or polysiloxane topcoat.	18-22

6.2.3 Atmospheric corrosion models

As presented in D2.2, the progress of atmospheric corrosion can be modelled in terms of thickness loss using a well-known power expression (Sommer et al. 1993, Radomski 2002).

$$C(t) = At^B \tag{6.1}$$

where, $C(t)$ is the uniform (measured as average over relatively small specimen surface areas) thickness loss (mm) after an exposure period of t years and coefficients A (mm/year) and B are empirical constants, obtained using regression analysis on physical test results grouped according to different atmospheric exposure conditions. This implies that the effect of the exposure conditions and type of metal (e.g. steel) are modelled implicitly by Equation 6.1 using suitable values for coefficients A and B. The recommended values for A and B are often deemed to exhibit high uncertainty, partly as a result of databases in which exposure conditions are poorly defined or poorly grouped. Over the years, attempts have been made to develop models to directly correlate the variables which determine the exposure conditions (e.g. relative humidity, SO_2, etc.) with the observed corrosion losses (Feliu et al. 1993, Klinesmith et al. 2007, EN ISO 9223 2012); these models are known as dose response functions (DRF). For instance, EN ISO 9223 (2012) recommends the use of a DRF for the calculation of coefficient A, in conjunction with the exposure classification system presented in Table 6-1:

$$A = 1.77SO^{0.52}\exp\left(0.020RH + f_{\mathrm{St}}\right) + 0.102CL^{0.62}\exp\left(0.033RH + 0.040T\right) \tag{6.2}$$

with $$f_{\mathrm{St}} = 0.150\left(T - 10\right) \text{ for } T \leq 10\ ^{\circ}\mathrm{C} \tag{6.3a}$$

otherwise $$f_{\mathrm{St}} = -0.054\left(T - 10\right) \tag{6.3b}$$

where, SO [mg/(m^2.d)] is the annual average deposition rate of sulphur dioxide, RH (%) is the annual average relative humidity, CL [mg/(m^2.d)] is the annual average deposition rate of chlorides and T ($^{\circ}$C) is the annual average temperature. For the coefficient B in Equation 6.1, EN ISO 9224 (2012) suggests a mean value μ_B = 0.523 with a standard deviation σ_B = 0.026. It has also been suggested that Equation 1 is suitable for periods up to 20 years; for t > 20 years thickness loss due to corrosion should be calculated using Equation 6.4 (EN ISO 9224 2012).

$$C(t > 20) = A\left[20^B + B\left(20^{B-1}\right)\left(t - 20\right)\right] \tag{6.4}$$

6.3 Framework for deterioration modelling

In this section, a framework for deterioration modelling of the coating-steel substrate system is presented, which is in line with the exposure classification recommendations of EN ISO 9223 (2012). Corrosion will begin to affect exposed steel surfaces immediately if no coating is applied, or after some time if coating has been applied, in places where the coating becomes ineffective. In other words, where a protective system is provided (which most often is the case) there will be a delay in the corrosion initiation in the substrate metal. The coating itself will gradually deteriorate with time (i.e. the protected steel surface area reduces with time) and eventually it will become completely ineffective. The time-dependent coating performance is modelled using information available in Network Rail standards where a

range of expected life (T_L) values are provided for a number of coatings used in the UK (see NR 2009a, b and c).

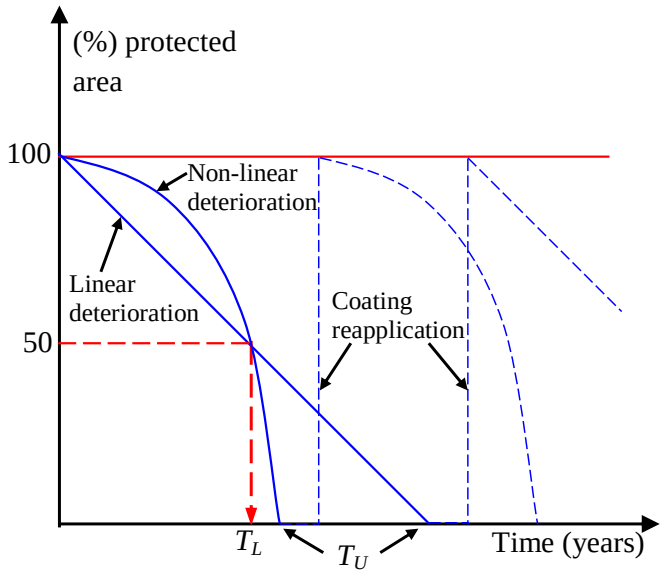

Figure 6-2 Deterioration model for coating system

A simple polynomial model (Equation 6.5) is developed, based on the assumption that 50% of the coated steel area will become unprotected at time T_L, shown schematically in Fig. 6-2.

$$\frac{A_{pr}(t)}{A_{pr0}} = 1 - \left(\frac{0.6t^2}{T_L^2} - \frac{0.1t}{T_L} \right) \qquad (6.5)$$

where, $A_{pr}(t)$ and A_{pr0} are the residual and initial protected area, respectively and t is the time in years. This model is used to predict the time T_U at which the entire coating is lost (and hence the entire underlying steel surface is actively corroding). Note that $A_{pr}(t) \leq A_{pr0}$ for all t and $A_{pr}(t) = 0$ for $t > T_U$.

This time-dependent coating performance model can be used to estimate the loss of thickness over any given surface (e.g. the web panel of a plate girder), assuming that coating breakdown becomes progressively more rapid, hence affecting the entire substrate area. Moreover, it can be coupled with structural resistance models to obtain performance ratios for different element types (Prucz & Kulicki 1998). For example, provided that local buckling does not become critical, the bending and shear resistance ratios – given by Equations 6.6 and 6.7, respectively – can be used to evaluate the time-varying performance of corroding bridge elements.

$$R_{BR}(t) = \left[\frac{M(t)}{M_0} \right] 100 \qquad (6.6)$$

$$R_{SR}(t) = \left[\frac{t_w(t)}{t_{w0}} \right] 100 \qquad (6.7)$$

where, $R_{BR}(t)$ (%) is the bending capacity ratio, M_0 and $M(t)$ are the initial and the time-varying moment capacities respectively, $R_{SR}(t)$ (%) is the shear capacity ratio and t_{w0} and $t_w(t)$ are the thicknesses of the uncorroded and corroded web elements respectively. Herein, for the calculation of the bending resistance at time t, it is assumed that the induced corrosion

damage is spread uniformly across the width of the flanges and the web depth. However, for particular cases it is also possible to adapt this equation to reflect the situation (observed in real cases) where the bottom flange suffers more than the top flange due to local water entrapment, bird fouling, etc. If buckling is of concern, the corresponding ratios for elastic global (EB) and local buckling (LB) can be taken as

$$R_{EB}(t) = \left[\frac{I(t)}{I_0}\right] 100 \qquad (6.8)$$

$$R_{LB}(t) = \left[\frac{t_{fl}(t)}{t_{fl,0}}\right]^2 100 \qquad (6.9)$$

However, structural elements carrying compressive loads may also be designed in the intermediate and stocky slenderness range, where yielding plays an increasingly important role. For these cases, the cross-sectional area becomes the controlling parameter and the relevant performance ratio, which is also applicable for tension members, becomes

$$R_A(t) = \left[\frac{A_{st}(t)}{A_{\mathrm{st},0}}\right] 100 \qquad (6.10)$$

where, $I(t)$ is the second moment of area around the bending axis of the corroding girder, $t_{fl}(t)$ is the thickness of the corroding compressive flange and $A_{st}(t)$ is the remaining cross-sectional area of the corroding girder with I_0, $t_{fl,0}$ and $A_{st,0}$ corresponding to the uncorroded girder.

6.4 Case study: A short-span railway bridge

6.4.1 Bridge description

In this section, performance profiles are presented for the external main girders of a typical short-span (half-through) railway bridge with a span of 9.6m as shown in Figure 6-3. The selected bridge consists of different element types, including external/internal main girders, stringers and cross-beams. The external main girders have 13mm thick top and bottom flanges while their web thickness is 10mm. The overall height of the section is 1220mm. The yield strength of the bridge is taken as f_y = 300 MPa. The two coating types described in Table 6-2 are examined, together with the case where no coating is applied. It is assumed that the protective coating is initially applied and no coating re-application takes place during the examined 70-year period.

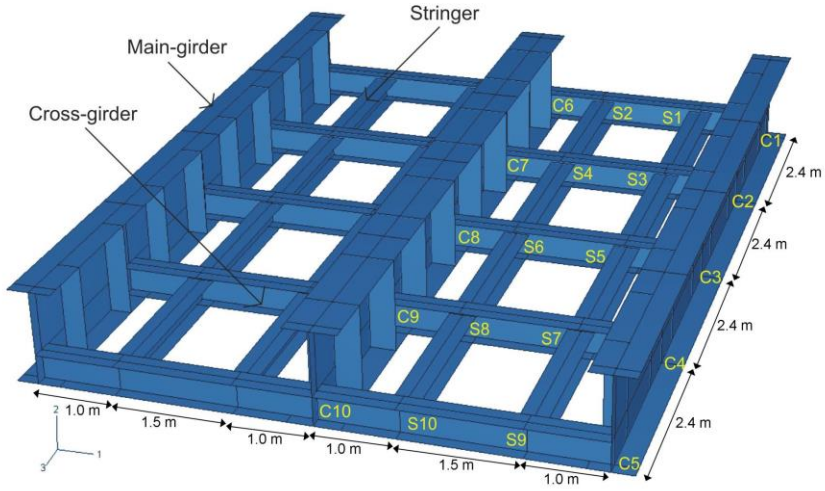

Figure 6-3 Schematic global view of the bridge

6.4.2 Exposure classification of bridge elements

As discussed earlier, the location of the aforementioned elements (i.e. internal/external) influences the aggressiveness of the microclimate to which their metal surfaces are exposed. To account for this, it is assumed in this example that the exposure conditions faced by internal elements are less harsh compared to external elements. It follows that the global exposure classification matches the microclimate of external elements (e.g. see external main girders in Figure 6-1), while internal elements (e.g. stringers) are assumed to be exposed to microclimates of lower aggressiveness. This assumption can be further refined, should particular factors prevail that may distinguish sub-elements of a girder, either in a vertical direction (e.g. top vs. bottom flange) or horizontally (e.g. end vs. middle sections).

6.4.3 Analysis cases

Initially, the corrosion models predictions of Equation 6.1 and 6.4 are examined for a number of exposure scenarios using the corrosivity categories of EN ISO 9223 (2012). Subsequently, a number of scenarios – summarised in Table 6-3 – are considered to investigate the influence of coating type and environment on the performance profile of the bridge elements.

Table 6-3 Analysis cases for the external main girder of the examined bridge (see also Table 6-1)

Name	Yield strength (MPa)	Coating		Corrosion model	
		Coating type	Service life, T_L (years)	Coefficient A (mm)	Coefficient B
EGC2NCu	300	No coating	-	0.0250	0.575
EGC2M274u	300	M27.4	7	0.0250	0.575
EGC2M21u	300	M21	22	0.0250	0.575
EGC5NCu	300	No coating	-	0.2000	0.575
EGC5M274u	300	M27.4	5	0.2000	0.575
EGC5M21u	300	M21	18	0.2000	0.575

6.5 Performance profiles

6.5.1 Corrosion losses over time

Figures 6-4a to 6-4c show predictions of the corrosion model given by Equations 6.1 and 6.4 for $t < 20$ and $t > 20$ years, respectively, for a number of exposure scenarios. In all cases, the values for coefficient *A* are obtained from the guiding values of EN ISO 9223 (2012); these are also summarised in Table 6-1 in this report. In Figures 6-4b and 6-4c, the upper bound of the ranges in Table 6-1 are used for coefficient *A*. In Figures 6-4a and 6-4b, a constant value (0.523) is used for coefficient *B*, which is the mean value for *B* suggested by EN ISO 9224 (2012). The effect of increasing *B* on the predicted thickness losses over time can be seen in Figure 6-4c where a higher *B* (0.575) is used (being the mean plus two standard deviations).

The results in these figures indicate that for corrosivity categories C1 to C4 the predicted corrosion losses are up to about 1mm during a 70 year period, if no protective system is applied (e.g. coating). On the other hand, much higher losses are predicted for corrosivity category C5. It should be noted that as an alternative to the values of Table 6-1, Equation 6.2 could be used to estimate coefficient *A*; this, however, would require the availability of sufficient information on the climatic conditions and levels of pollution for a specific area.

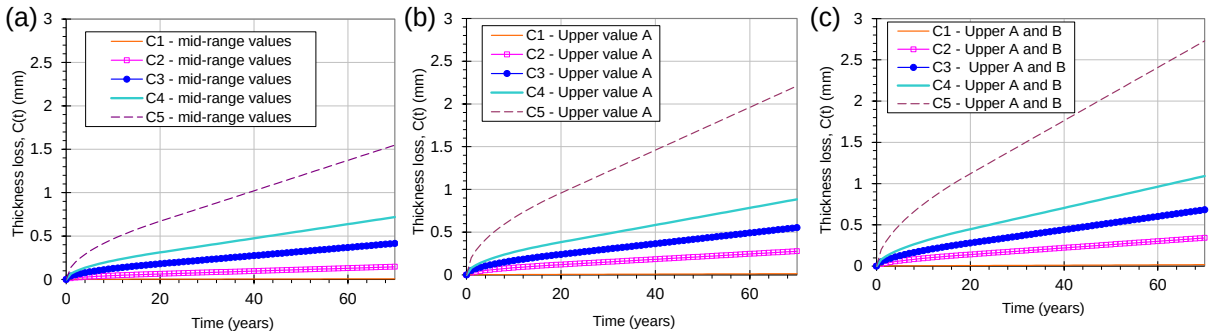

Figure 6-4 Thickness loss over time predicted using Equation 6.1 and Table 6-1: (a) mid-range value for A and B = 0.523, (b) upper limit for A and B = 0.523 and (c) upper limit for A and B = 0.575

6.5.2 Coating performance over time

Figure 6-5 shows the effect of atmospheric corrosivity on the evolution of (normalized) coating performance (Equation 6.5) over time for the two coating systems used (see Table 6-2). The results indicate that the influence of atmospheric corrosivity for the M27.4 coating, which is recommended for patch repairs, is relatively small but noticeable. As shown in Figure 6-5, the influence of corrosivity harshness is small for the initial 10 years of exposure for coating system M21. Beyond this point, the increased corrosivity of C5 environment caused an approximately 5 year reduction in the ultimate coating life T_U (i.e. time at which the protection provided by the coating is lost entirely) compared with the predicted T_U in the less corrosive environment C2.

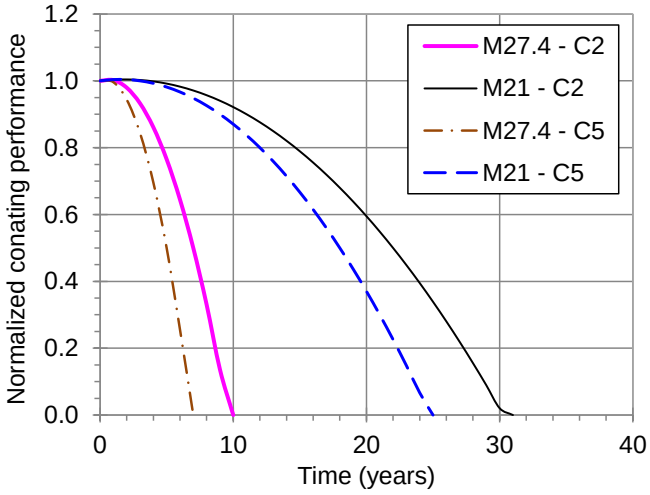

Figure 6-5 Effect of atmospheric corrosivity on the performance evolution of different coatings

6.5.3 Performance profiles for the external main girder

Figures 6-6 and 6-7 show the thickness losses over time for the flanges and web, respectively, of the external main girder for the different scenarios examined (Table 6-3). The case where no coating is applied to the girder is also shown. The results indicate that the harshness of atmospheric corrosivity has the highest influence on the evolution of thickness reduction in both flanges and web. The thickness losses for exposure C2 (rural environment) are much lower compared to the much more aggressive industrial environment C5. The results indicate that the influence of the coating was relatively small for the less corrosive environment C2. In contrast, the results in Figures 6-6 and 6-7 show that the type of coating system has a significant effect on the evolution of residual thickness in the flanges and web; this however depends on the coating system used. This can be explained by considering the delay in the corrosion initiation caused by the high performance coating system M21. This effect is much smaller when the less effective bitumen-based M27.4 is used.

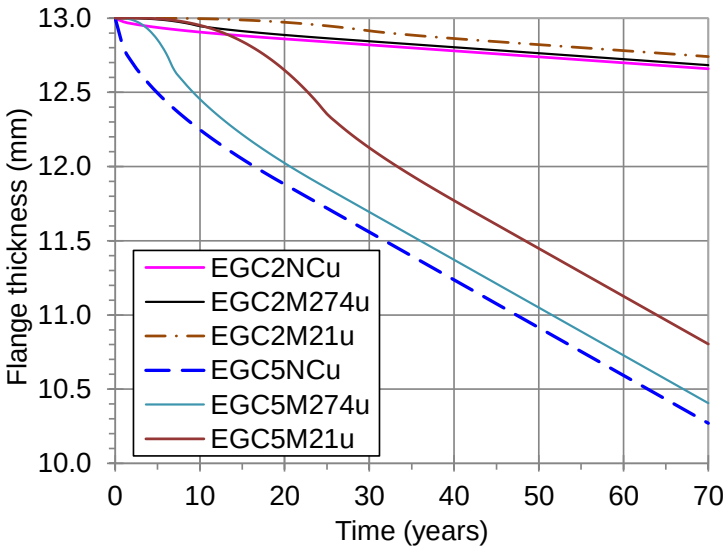

Figure 6-6 Loss of flange thickness over time for the different scenarios examined (see Table 6-3)

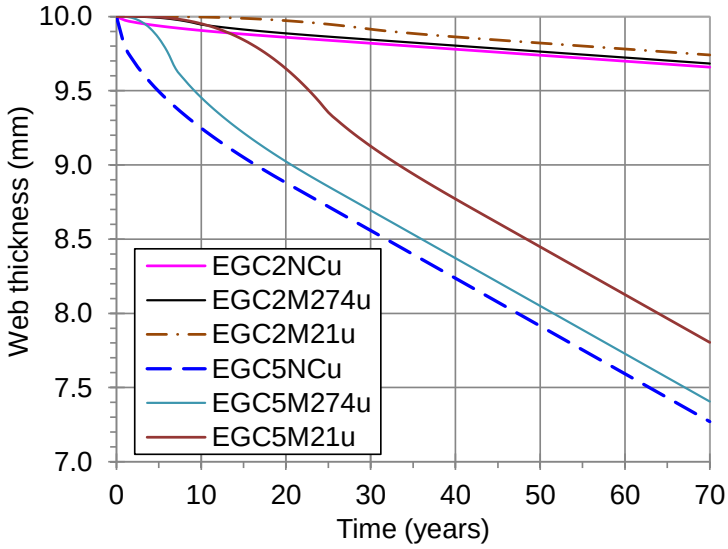

Figure 6-7 Loss of web thickness over time for the different scenarios examined (see Table 6-3)

So far, the performance profiles have been related to the performance of the coating and any subsequent thickness loss, without paying attention to the structural consequences of these effects. In this context, the profiles shown in Figure 6-6 and 6-7 are primarily related to condition. Moving to capacity-based (or resistance-based) performance profiles, Figures 6-8 and 6-9 depict the evolution of bending and shear performance ratios, respectively, for the case of the external main girder. The results indicate that there is a small decrease of bending resistance for the cases where low atmospheric corrosivity (i.e. C2) is assumed. In these cases, the performance of the coating system has a small overall effect on the predicted response. Similar results are obtained for the shear capacity factors of the cases with exposure classification C2.

Moreover, the results show that the harsh exposure conditions associated with the C5 corrosivity category have a significant effect on the rate of performance deterioration in bending and shear. It is interesting to note that, in all cases examined, the high performance coating M21 provides sufficient protection for the first quarter of the 70 year period and small differences are observed between the girders exposed to different environments.

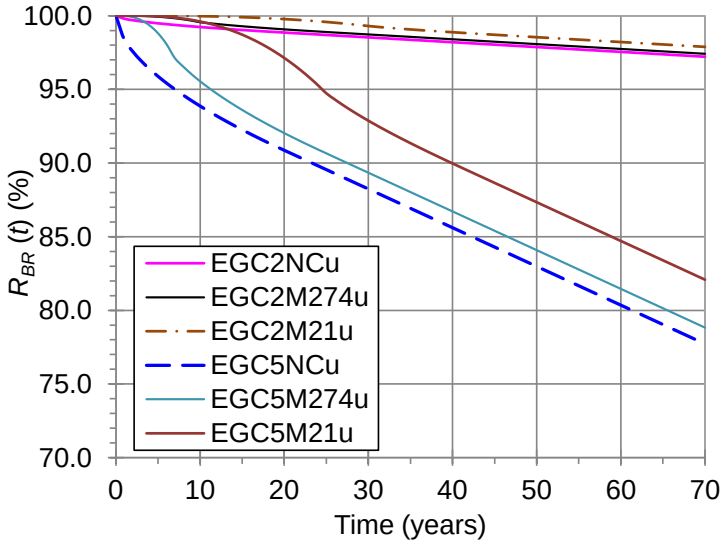

Figure 6-8 Evolution of external main girder bending capacity factors for the different scenarios examined (see Table 6-3)

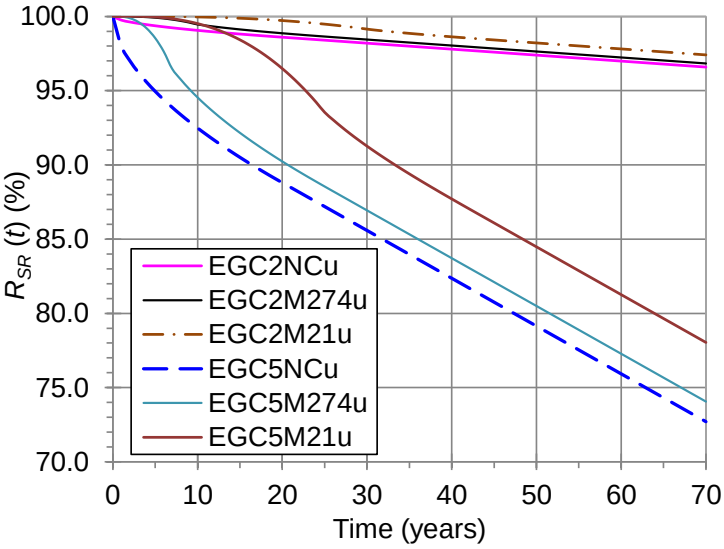

Figure 6-9 Evolution of external main girder shear capacity factors for the different scenarios examined (see Table 6-3)

6.6 Conclusions for metallic bridges

In this chapter, a methodology was presented for the development of condition and capacity profiles for deteriorating steel elements – affected by atmospheric corrosion – including the coating performance and its gradual breakdown over time. The following conclusions can be drawn from this investigation:

1. The harshness of atmospheric corrosivity has a significant effect on both the performance of the protective coating system, as well as the long-term corrosion thickness losses.
2. The type and performance of the coating system has a small effect on the predicted response of elements exposed to low corrosivity (C2) environments. In contrast, in highly corrosive atmospheres, the coating can provide sufficient corrosion protection for several years. Once the coating becomes ineffective in protecting against atmospheric corrosion, the rate of deterioration is determined by the harshness of the exposure conditions.
3. The methodology that has been developed can account for a wide range of exposure conditions, corresponding to the classification provided in a recent international standard. It is adaptable so as to cater for micro-climate effects both at inter-element level and within a single element.
4. Depending on policy, budget and maintenance constraints, ageing metallic bridges may have to be managed either on a condition or a capacity basis. The developed methodology has the flexibility to enable such decisions to be made, based on relatively simple models developed for a wide range of exposure conditions and coating systems.
5. The methodology was demonstrated through a simple case study in which performance profiles for a typical short-span bridge were developed. Both the case of a coated and an uncoated structure were presented for illustration purposes.

6.7 References

Czarnecki, A.A. & Nowak, A.S. 2008. Time-variant reliability profiles for steel girder bridges. Structural Safety 30:49-64.

EN ISO 12944-5. 1998. EN ISO 12944-5 – Paints and varnishes – Corrosion protection of steel structures by protective paint systems – Part 5: Protective paint systems.

EN ISO 9223. 2012. EN ISO 9223:2012 – Corrosion of metals and alloys – Corrosivity of atmospheres – Guiding values for the corrosivity categories.

EN ISO 9224. 2012. EN ISO 9224:2012 – Corrosion of metals and alloys – Corrosivity of atmospheres - Classification, determination and estimation.

Feliu, S., Morcillo, M. & Feliu, S. Jr. 1993. The prediction of atmospheric corrosion from meteorological and pollution parameters – I. Annual corrosion. Corrosion Science 34(3), 403-14.

Gascoyne, A. & Bottomley, D. 1995. Atmospheric corrosion rates of railway bridge structures. Report No. LR-MSU-084. Issued by Scientifics for the British Rail Research, British Railways Board.

Hutchins, J.S. & McKenzie, M. 1973. Characterisation of bridge locations by corrosion and environmental measurements – first year results. Rept No.LR550, Transport and Road Research Laboratory. UK.

Kayser, J.R. & Nowak, A.J. 1989. Capacity loss due to corrosion in steel-girder bridges. Journal of Structural Engineering 115(6):1525-37.

Klinesmith, D.E., McCuen, R.H. & Albrecht, P. 2007. Effect of environmental conditions on corrosion rates. Journal of Materials in Civil Engineering 19(2):121-29.

Landolfo, R., Cascini, L. & Portioli, F. 2010. Modeling of metal structure corrosion damage: a state of the art report. Sustainability 2:2163-75. doi:10.3390/su2072163.

NR. 2009a. NR/L3/CIV/002: The use of protective coatings and sealants. Guidance Note. Network Rail, UK.

NR. 2009b. NR/L3/CIV/039: Level 3 – Specification for the assessment and certification of protective coatings and sealants. Network Rail, UK.

NR. 2009c. NR/L3/CIV/040: Level 3 – Specification for the use of protective coating systems. Network Rail, UK.

Prucz, Z. & Kulicki, J.M. 1998. Accounting for effects of corrosion section loss in steel brides. Transportation Research Record 1624:101-9. Paper No.98-0933.

Radomski, W. 2002, Bridge rehabilitation, Imperial College Press.

Sharifi, Y. & Paik J.K. 2011. Ultimate strength reliability analysis of corroded steel-box girder bridges. Thin-Walled Structures 49:157-66.

Sommer AM, Nowak AS, Thoft-Christensen P. Probability-based bridge inspection strategy. Journal of Structural Engineering, ASCE 1993;119:3520–36.

Sorensen, P.A., Kiil, S., Dam-Jojansen, K. & Weinell, C.E. 2009. Anticorrosive coatings: a review. J. Coat. Technol. 6(2):135-76.

Tamakoshi, T., Yoshida, Y., Sakai, Y. & Fukunaga, S. 2006. Analysis of damage occurring in steel plate girder bridges on national roads in Japan. In 22nd US–Japan Bridge Engineering Workshop. Seattle. WA.

7. Concrete Tunnels

7.1 Introduction

This chapter presents the development of time-variant performance profiles concerning concrete lined tunnels based on deterioration models which take into account time evolution, as identified in deliverable D2.2.

It is worth clarifying the notion of *performance*, as will be employed herein. Two points of view can be considered: the first one consists in assessing the performance of an asset through its capacity level (e.g. traffic or load level that it can support) and the second one consists in assessing its physical condition. Degradation mechanisms can imply a loss of capacity, condition or both (conversely, interventions can imply an increase). With regard to tunnels, it seems difficult to consider capacity performance evolving with time; this is why only condition will be tackled in this chapter. The condition performance refers to the state of an asset which can possibly be degraded. Consequently there are as many performance indicators as mechanisms of degradation, assuming that they are all uncoupled for the sake of simplicity and applicability. For every mechanism, the performance indicator aims at quantifying how far the asset is from a limit state. The latter corresponds either to a resistance mode or to a conventional threshold. If we consider a precise mechanism and formally denote *S* as the level of action responsible for the degradation and *R* the resistance or threshold such that $S \leq R$ corresponds to an acceptable state, the following definition of the performance *P* is proposed:

$$P = 1 - \frac{S}{R} \qquad (7.1)$$

This definition implies that the performance can be seen as the distance between the resistance and the action normalized by the resistance. This means that the performance is 1 when the action in non-existent, decreases when the action increases but remains positive as long as the criterion is not reached. The value 0 corresponds then to the activation of the degradation mechanism.

Among the degradation phenomena that could affect a tunnel performance, it has been chosen in D2.2 to focus on deterioration mechanisms of the lining material (concrete in this chapter) and to disregard accidental damage (vehicle impacts, fire…). The principal causes of deterioration in concrete lined tunnels have been identified:

- Steel reinforcement corrosion
- Sulphate attack
- Alkali-aggregate reactions
- Freeze-thaw attack

Many details about the description, origins and consequences of those phenomena can be found in D2.2, some of which will be recalled when needed in the present deliverable. In addition, D2.2 also covers intervention strategies from a qualitative point of view.

The chapter of D2.2 dedicated to tunnels concludes by noting that even though many models have been developed to estimate the effects of different deterioration mechanisms on the asset state, there is still a lack of models which take time into account in a simple way, especially concerning sulphate attack, alkali-aggregate reactions and freeze-thaw attack. Consequently, the following sections focus on the degradation of concrete due to the corrosion of steel rebars, for which simple models are available. Thus, only tunnels lined with reinforced concrete are concerned.

Keeping in mind the objective of taking advantage of performance models to implement a LCA tool in WP5 in the form of a spreadsheet, it is clear that the models should remain as simple as possible, which disqualifies models relying on heavy numerical calculations (e.g. finite element or finite volume models) or involving coupled mechanisms. Hence, analytical expressions are favoured in the following even if their applicability can be limited to idealised situations or specific types of asset. Input variables needed for the models are presented, as well as any assumptions regarding the applicability conditions. Possible modifications of the profiles, by taking into account interventions, are finally briefly evoked although quantitative models allowing partial recovery of the performance are still lacking.

7.2 Deterioration mechanisms related to steel reinforcement corrosion

As already highlighted in D2.2, the deterioration of reinforced concrete is not immediately observable from the beginning of the structure's life even under harmful conditions. Indeed, two time periods can be identified (see Figure 7-1 extracted from D2.2):

- An initiation period during which the structure remains undamaged. This period corresponds to a phase of incubation. The steel rebars are not affected by corrosion yet but aggressive agents (principally carbon dioxide or chloride ions depending on the exposure conditions) progressively penetrate into the concrete until the propagation front (of carbonation or chloride ion presence) reaches the rebars. The propagation front is defined by a critical value which triggers steel corrosion. In the case of carbonation, an increase of dissolved CO_2 concentration implies a reduction of pH of the interstitial fluid (normally around 13 for a sound concrete) which induces steel depassivation (pH around 9) and eventually steel reinforcement corrosion. In the case of chloride ion ingress, the depassivation phenomenon leading to corrosion is localised and characterized by the formation of pits. For more detailed information about these chemical processes, one can refer to the literature identified in D2.2 or to the guide (AFGC 2007).

- A propagation period starting from the corrosion process. This period can be divided in three sub-periods as shown in Figure 7-1: a first one during which the corrosion product volume increases while the rebar section decreases until cracking occurs in concrete and steel-concrete bonds break, a second one leading to concrete spalling and a third one during which the previous deterioration mechanisms increase until reaching a failure criterion of the structure.

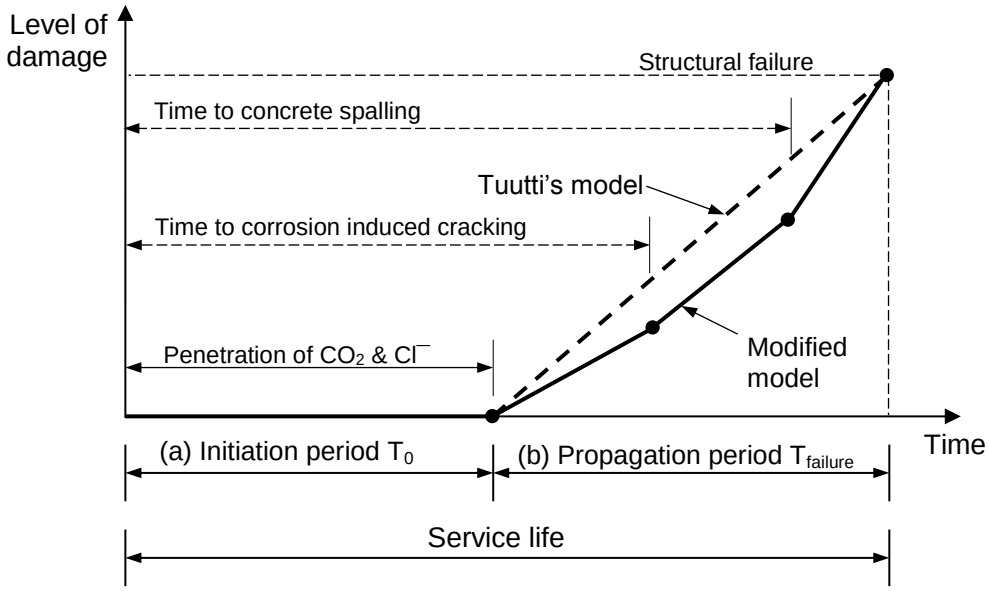

Figure 7-1 Service-life models of a corroding RC structure (D2.2 citing Otieno 2011): (a) Initiation and (b) propagation stages

7.3 Development of performance profiles

From a rigorous point of view, the performance of the structure is not actually affected during the initiation period. Furthermore the concrete cover could even be improved in the case of carbonation during an initial period. Indeed the precipitation of $CaCO_3$ fills the pores of the cement phase, increasing the strength and decreasing the transfer properties of concrete, in other words creating an obstacle to the propagation of the carbonation front. The loss of performance will occur more or less rapidly when the front reaches the rebars. As a consequence, a performance index should *a priori* be calculated from quantitative elements of the propagation phase (corrosion products, loss of steel section, loss of mechanical properties…).

As mentioned in D2.2, referring to the approach outlined in the CONREPNET project (CONREPNET 2001), the through-life management of concrete structures could be improved by considering proactive interventions instead of reactive ones according to global cost and duration of disruption criteria. Hence, the possibility to assess the state of the structure in terms of aggressive agent penetration during the initiation period becomes crucial. That is why it is proposed here to build not only a performance indicator based on the condition of the structure and related to the corrosion level (structural performance in Fig.2) but also an indicator allowing to assess how far the structure is from corrosion initiation (performance against depassivation in Figure 7-2). This reasoning is, of course, valuable only if conditions for steel corrosion after depassivation are actually met (especially the presence of both oxygen and water in the vicinity of rebars). Figure 7-2 shows the interest of following both the two indicators for a structure manager to decide between a reactive or a proactive strategy.

In the reactive strategy, the interventions are carried out only in presence of observable damage to concrete. Several types of intervention are described in D2.2: crack and spall repair of concrete, replacement of steel rebars, structural injection of cracks, segmental lining repair. More details can be found in (AFGC 2003) which also describes the cathodic

protection as an electrochemical treatment to protect steel against corrosion possibly coupled with concrete cover repair. Their cost may be important and D2.2 points out the problems that can arise if the repair technique and the possible collateral damage induced by bad applications are not perfectly understood. Moreover, these types of intervention can be long lasting, which may have consequences for the proper functioning of the tunnel.

In the proactive strategy, interventions are carried out to prevent the front of aggressive agents responsible for steel depassivation from reaching the rebars. Hence the concrete lining is still intact but the interventions aim at postponing the initiation of corrosion if the latter is likely to occur. The main technique described in (AFGC 2003) consists in electrochemical treatments such as realkalisation (increasing the pH) in the case of a carbonated concrete and chloride extraction.

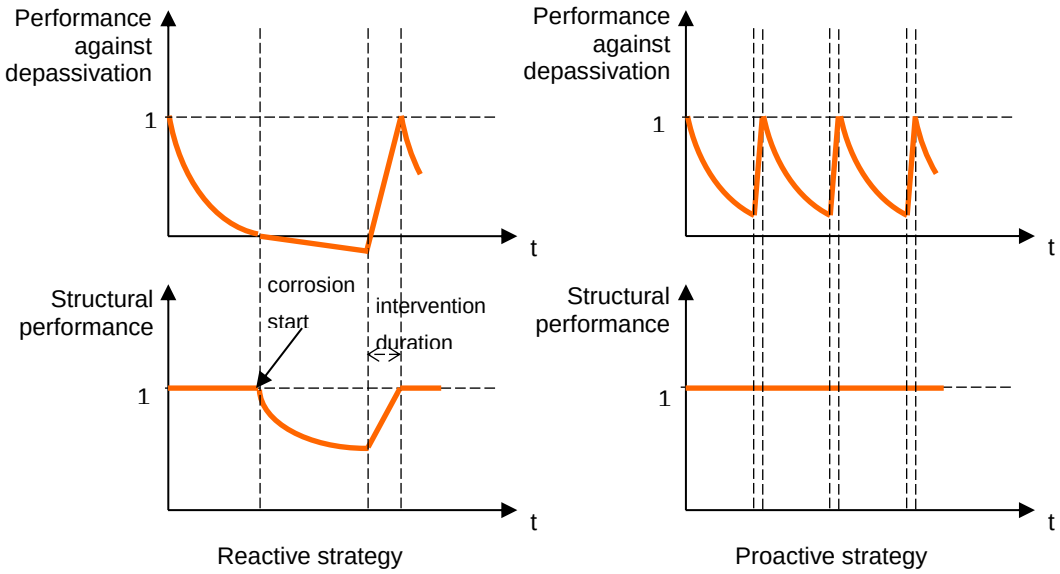

Figure 7-2 Combined performance profiles for steel corrosion and application to reactive and proactive strategies

7.4 Performance profile for depassivation induced by carbonation

As already mentioned, the carbonation process corresponds to an acid-base chemical reaction between dissolved carbon dioxide and hydrates contained in the cement paste. This reaction decreases the pH of the interstitial solution inducing consequently the depassivation of steel. The motion of carbon dioxide molecules, coming from the boundary of the structure and feeding the reaction, is assumed governed by a diffusion law (Fick) within the gaseous phase. This coupled mechanism between chemical reactions and transport is made even more complex because of the influence of many parameters (concrete formulation and microstructure, temperature, initial conditions, time-varying boundary conditions) and the modifications of the microstructure induced by the chemical reactions and subsequently of the macroscopic material properties such as the diffusivity. This complexity makes it rather difficult to estimate precisely and in a simple way the carbonation front depth $X_c(t)$ i.e. the distance from the boundary where the pH equals the critical value for steel depassivation

(about 9). Empirical as well as more or less sophisticated chemo-physical models allowing to estimate $X_c(t)$ have been developed in the literature (Thiery 2005, AFGC 2007). A complete review of parameters, assumptions and domains of validity of chemo-physical models is presented in (AFGC 2007, chap. 10, table 16). The simplest analytical model is in the form:

$$X_c(t) = K\sqrt{t} \qquad (7.2)$$

where K is a parameter depending on both the composition and the microstructure of the concrete (w/c ratio, binder content and type, morphology of the granular assemblage,…) and the environmental conditions (relative humidity, temperature, pressure, initial and boundary conditions of CO_2…).

A first approach consists in estimating K through a measurement of the carbonation front depth at a given time t by means of a coloured indicator such as phenolphthalein for which the pH transition from pink to colourless is about 9 (RILEM Draft Recommendation, CPC-18 1984, CEN Report 2003, EN 14630 2007). This method requires core sampling (destructive test).

A second approach consists in taking advantage of models expressing K in (Eq. 7.2) as an explicit function of material and environmental parameters. Among the available models, the one developed in (Papadakis 1991a, 1991b, 1991c) is chosen for the sake of simplicity. In this model, the carbonation front depth is obtained under the form (Eq. 7.2) with:

$$K = \sqrt{\frac{2D_{CO_2}[CO_2]^0}{n^0_{Ca(OH)_2} + 3n^0_{CSH} + 3n^0_{C_3S} + 2n^0_{C_2S}}} \qquad (7.3)$$

where D_{CO_2} is the effective diffusion coefficient of carbon dioxide in the carbonated region (in m^2/s), $[CO_2]^0$ is the concentration of carbon dioxide in the outside air (i.e. at the boundary of the lining) per unit volume of the gas phase (in mol/m^3) and n^0_i is the apparent initial concentration of compound i (i.e. moles per unit volume of concrete in mol/m^3).

This model relies on several simplifying assumptions : the progressive modifications of the porous space due to chemical reactions are disregarded, no moisture gradient and no relative humidity evolution are taken into account, D_{CO_2} is uniform and constant (as a consequence of the preceding assumptions), no carbon dioxide is present in the material at the initial time, the initial content of Portlandite and other reactive minerals is uniform and the chemical reactions of carbonation are much faster than the diffusion process. The resolution of the equation system composed of mass balance, Fick law, chemical kinetics and initial and boundary conditions leads to a sharp carbonation front separating two zones: a completely carbonated zone towards the boundary of the structure and a zone which remains uncarbonated and even totally free of carbon dioxide.

Equation (7.3) is often simplified by neglecting the minerals other than Portlandite:

$$K = \sqrt{\frac{2D_{CO_2}[CO_2]^0}{n^0_{Ca(OH)_2}}} \qquad (7.4)$$

Based on the assumption that Portlandite plays a more important role than other minerals in the carbonation process from a thermodynamic and kinetic point of view, the interest of the simplified form (Eq. 7.4) is that it minimizes the number of required parameters. Moreover, it tends to overestimate the carbonation depth, which is rather conservative with regard to corrosion risk.

The practical use of (Eq. 7.4) requires an estimation of all the quantities at stake:

- $[CO_2]^0$ in normal conditions can be taken as 0.013mol.m^{-3}, corresponding to an environment containing 0.03% in volume of CO_2 at 20°C, this value can of course be modified under precise circumstances (e.g. a tunnel through which diesel locomotives pass),
- $n^0_{Ca(OH)_2}$ can be measured by thermogravimetric or chemical analysis (AFGC 2007) or can be estimated by a model. Several more or less simple models exist in the literature depending on assumptions made on the hydration process. For example, assuming that only the C_3S hydration reaction produces calcium hydroxide, (AFGC 2007) gives for a CEM I at 28 days :

$$n^0_{Ca(OH)_2} = \sup(0\,;\, c\times f_{C_3S}\times \inf(1,(w/c)/0.418)\times 0.422 - s\times 0.617)/M_{Ca(OH)_2} \quad (7.5)$$

  where c is the cement content per unit volume of concrete in kg.m^{-3}, f_{C3S} is the ratio of C_3S within the cement, w/c is the water-cement mass ratio, s is the silica fume or pozzolanic mineral addition content per unit volume of concrete in kg.m^{-3} and $M_{Ca(OH)_2}$ is the molar mass of calcium hydroxide (0.074kg.mol^{-1}).
- D_{CO_2} is probably the most complex parameter to estimate since it depends on the morphology of the porous phase as well as on the saturation degree (in relation with the relative humidity) and the temperature. As an initial approximation, the formula provided in (Papadakis 1991b) can be used:

$$D_{CO_2} = 1.64\times 10^{-6}\times \phi_p^{c\,1.8}\times (1-RH)^{2.2} \quad (7.6)$$

  where RH is the relative humidity and ϕ_p^c is the porosity of the carbonated paste (hydrated cement+water) in the concrete. The latter can be related to the porosity of carbonated concrete ϕ^c by means of the relationship (Papadakis 1991b):

$$\phi_p^c = \phi^c\left(1+\frac{\frac{g\rho_c}{c\rho_g}}{1+\frac{w\rho_c}{c\rho_w}}\right) \quad (7.7)$$

  with g, c and w respectively the weights of aggregates, cement and water per unit volume of concrete and ρ_g, ρ_c and ρ_w the corresponding respective densities. In a first approach, the porosity ϕ^c can be identified to the porosity of the sound concrete ϕ if the variation of porosity due to carbonation of the hydrates is neglected. To take the latter into account, (Papadakis 1991a) proposes the following relationship:

$$\phi^c = \phi - \left(n^0_{Ca(OH)_2}\times \Delta v_{Ca(OH)_2} + n^0_{CSH}\times \Delta v_{CSH}\right) \quad (7.8)$$

where the variations in molar volumes due to respectively $Ca(OH)_2$ and CSH carbonations are given by

$$\Delta v_{Ca(OH)_2} = 3.85\times10^{-6}\, m^3.mol^{-1} \quad ; \quad \Delta v_{CSH} = 15.39\times10^{-6}\, m^3.mol^{-1} \qquad (7.9)$$

The criterion of depassivation of the steel rebars is given by the equality between the depth of carbonation $X_c(t)$ (Eq. 7.2) and the thickness of the concrete cover denoted by c_p. According to (Eq. 7.1) in which $X_c(t)$ plays the role of the action S and c_p plays the role of the resistance R, the performance indicator against depassivation becomes:

$$P_{dep}(t) = 1 - \frac{X_c(t)}{c_p} = 1 - \frac{K\sqrt{t}}{c_p} \qquad (7.10)$$

From (Eq. 7.10), it is interesting to introduce the expected time T_{dep} for depassivation due to carbonation:

$$T_{dep} = \left(\frac{c_p}{K}\right)^2 \qquad (7.11)$$

7.5 Performance profile for depassivation induced by chloride ion ingress

Although railway tunnels may not be exposed to chloride ions as much as structures in contact with seawater or de-icing salts, depassivation due to these aggressive agents can still be encountered. Moreover, in the case of tunnels, chloride ions may come from both sides of the concrete lining, i.e. from the internal wall in contact with air and from the external wall in contact with the ground possibly saturated with a solution containing chlorides.

The aggressive action of chloride ions in contact with the steel rebars is different from that of carbon dioxide. Whereas the latter induce a pH decrease and a rather uniform production of corrosion, the former are not consumed in the oxidation-reduction between steel and oxygen but play the role of catalyst and induce localised corrosion (pits).

Two types of chlorides can be found in concrete: the free chlorides in ionic form in the interstitial solution and the chlorides bound to the solid phase (adsorbed or chemically linked in the cement matrix). Only the free ones play a role in the depassivation process since they can reach the steel rebars. Chlorides present in concrete may have been introduced during the mixing or may have penetrated from outside. The motion of chloride ions in concrete is controlled either by diffusion within the liquid phase (requiring then a high degree of saturation) or by capillary absorption and convection in the case of wetting-drying cycles. The latter are not considered in the following.

Among the models of chloride ion ingress reviewed in (AFGC 2007), the simplest one is based on Fick's second law. The free chloride concentration C=[Cl^-] in the interstitial solution is assumed to depend only on the time and the depth x from the concrete wall (invariance along the axes parallel to the wall). The second Fick's law implies that C is solution to:

$$\frac{\partial^2 C}{\partial t^2} = D^{app} \frac{\partial^2 C}{\partial x^2} \qquad (7.12)$$

where D^{app} denotes the apparent diffusion coefficient. The latter depends on the effective diffusion coefficient D^{eff} (itself depending on the intrinsic chloride diffusion coefficient in water, the porosity, the saturation degree and the tortuosity of the concrete microstructure), the porosity ϕ, the bulk density of concrete in dry state ρ as well as the slope of the chloride-matrix interaction isotherm $\partial m_b / \partial C$ relating the mass of bound chlorides per unit mass of dry solid m_b to the free chloride concentration :

$$D^{app} = \frac{D^{eff}}{\phi + \rho \frac{\partial m_b}{\partial C}} \qquad (7.13)$$

An analytical solution to (12) is obtained under simplifying assumptions : the structure is seen as a semi-infinite medium, the initial chloride concentration C_i is uniform, the chloride concentration C_o at the boundary *x=0* is constant and the apparent diffusion coefficient D^{app} is constant and uniform :

$$C(x,t) = C_o + (C_i - C_o)\,\mathrm{erf}\left(\frac{x}{2\sqrt{D^{app} t}}\right) \text{ with } \mathrm{erf}(u) = \frac{2}{\sqrt{\pi}} \int_0^u e^{-\xi^2}\,\mathrm{d}\,\xi \qquad (7.14)$$

The chloride ingress front can then be defined from (Eq. 7.14) with the aid of a critical chloride concentration, i.e. a concentration liable to initiate reinforcement corrosion. The initiation criterion often adopted is that based on the ratio for the free chloride to the hydroxide ions concentrations as proposed in (Hausmann 1967):

$$\frac{C}{[OH^-]} \geq 0.6 \text{ i.e. } C^{crit} = 0.6[OH^-] \qquad (7.15)$$

For an interstitial solution of pH=13, the critical chloride concentration is then equal to 0.06mol.l^{-1}. It is worth highlighting the possible interaction between carbonation and chloride ion ingress: Indeed, although carbonation is likely to decrease the diffusion coefficient and thus the velocity of chloride ions, it mainly decreases the pH and consequently, according to (Eq. 7.15), the critical value of chloride concentration leading to corrosion. As often mentioned in the literature, for a non-carbonated concrete, the critical value (Eq. 7.15) corresponds to a chloride mass concentration of approximately 0.4% relative to the cement mass. In addition, it should be noted that an extension of the critical concentration to other values depending on the w/c ratio, cement composition and thickness of cover can be found in (Fagerlund 2011).

Taking advantage of (Eq. 7.14) together with (Eq. 7.15) yields the following expression of the location of the chloride ingress front:

$$X_{chl}(t) = 2\sqrt{D^{app}}\,\mathrm{erf}^{-1}\left(\frac{C_o - C^{crit}}{C_o - C_i}\right)\sqrt{t} \qquad (7.16)$$

Whereas the equations governing the carbonation process and the chloride ion ingress are different, the front propagations (Eq. 7.2) and (Eq. 7.16), obtained by resolution under simplifying assumptions and often practically used, obey the same kind of rule in $\sqrt{t}$. Nevertheless, both theoretical and experimental results show some discrepancies with those rules, see for example (Thiery 2005) for carbonation. With regard to chloride ion ingress, one major criticism against (Eq. 7.16) relies on the fact that the assumption of constant and uniform diffusion coefficient should be questioned in presence of a zone of unsaturated concrete (where the chloride diffusion coefficient is lower), likely to exist near the boundary in contact with air, especially in the case of wetting-drying cycles. An adaptation of (Eq. 7.14) taking into account such a convection zone where the chloride concentration profile differs from the solution to Fick's second law can be found in (AFGC 2007): it consists in translating the origin the abscissa x at the depth Δx where the solution recovers the expression (Eq. 7.14) and replacing C_o by the concentration at depth Δx. However those new variables might be difficult to estimate practically except by identification of the actual profile on core samples. Another approach is to extrapolate the profile complying with Fick's second law to the boundary and consider that C_o plays the role of an equivalent surface concentration (see Figure 7-3).

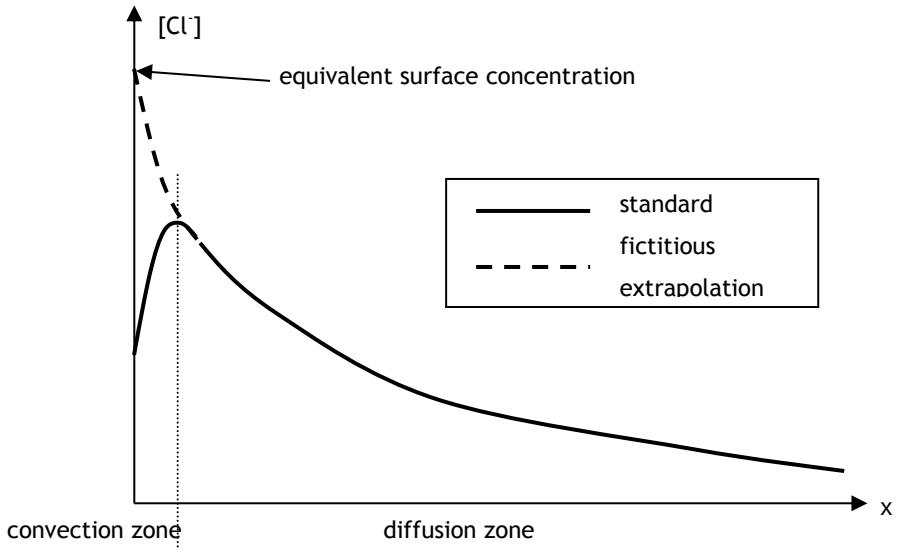

Figure 7-3 Chloride profile in a concrete subjected to wetting-drying cycles and extrapolation to the equivalent surface concentration

Although it may be difficult to assess the value of the equivalent surface concentration except by performing an actual chloride profile from the analysis of a sample core, typical values depending on the type of environment are suggested in (AFGC 2007): from 10 to 100g.l^{-1}, i.e. 0.28 to 2.8mol.l^{-1} since the chloride molar mass is 35.45g.mol^{-1}.

More realistic empirical models have been built by extension of (Eq. 7.16) in order to take into account the dependence of the diffusion coefficient on temperature, on interaction of ionic flows (coefficient α in (Eq. 7.17)) and on time since the microstructure of the cover concrete evolves with time (see a review in (Bioubakhsh 2011) and (AFGC 2007)). From those models the following expression of the chloride front can be built:

$$X_{chl}(t) = 2\sqrt{\alpha D^{app}(t)}\,\mathrm{erf}^{-1}\left(\frac{C_o - C^{crit}}{C_o - C_i}\right)\sqrt{t} \qquad (7.17)$$

with

$$\alpha = 1 + \frac{1}{4C_o} \quad (C_o \text{ in mol.l}^{-1}) \qquad (7.18)$$

$$D^{app}(t) = D_{ns(mig)}\left(\frac{t_0}{t}\right)^{a} \exp\left(b_e\left(\frac{1}{T^{ref}} - \frac{1}{T}\right)\right) \qquad (7.19)$$

where $D_{ns(mig)}$ corresponds to the apparent diffusion coefficient at the reference time t_0 and temperature T^{ref} obtained by a migration test in non-steady-state conditions on a core sample in laboratory (AFGC 2007, chap 7).

The temperature-dependence in (Eq. 7.19) relies on the Arrhenius equation where b_e is the Arrhenius constant, T^{ref} is the reference temperature (equal to 293K in laboratory conditions) and T is the temperature in K. A value of 4800K for the constant b_e is suggested in (AFGC 2007) and (Bioubakhsh 2011) citing (Lin 1993) proposes the following values with respect to 3 w/c ratios:

w/c ratio	0.4	0.5	0.6
b_e (K)	5016	5359	3830

The time-dependence in (Eq. 7.19) relies on the parameter a which is constant for a specific concrete (depending on mix composition). Values for a for all varieties of concrete are not well established but preliminary works cited in (Bioubakhsh 2011) give values in the range of 0.2 to 0.3 for normal Portland cement mixtures and higher values between 0.5 and 0.7 to fly ash and slag concrete.

In absence of information about the time-dependence of the diffusion coefficient, the coefficient α in (Eq. 7.19) can be taken as 0.

If no laboratory test can be performed, (Vu and Stewart 2000) proposes an empirical analytical expression which could possibly be taken as a constant apparent diffusion coefficient:

$$D^{app} = 0.15 D_{H2O}\left(\frac{1 + \frac{w\rho_c}{c\rho_w}}{1 + \frac{w\rho_c}{c\rho_w} + \frac{g\rho_c}{c\rho_g}}\right)\left(\frac{\frac{w\rho_c}{c\rho_w} - 0.85}{1 + \frac{w\rho_c}{c\rho_w}}\right)^3 \text{ with } D_{H2O} = 1.6\,10^{-9}\,m^2 s^{-1} \qquad (7.20)$$

Finally the performance indicator against depassivation can be built similarly to that in the case of carbonation (Eq. 7.10):

$$P_{dep}(t) = 1 - \frac{X_{chl}(t)}{c_p} \qquad (7.21)$$

If the time dependence of the diffusion coefficient is taken into account ($a \neq 0$) the value of the time at which depassivation occurs results from the resolution of the nonlinear equation:

$$P_{dep}(T_{dep}) = 1 - \frac{X_{chl}(T_{dep})}{c_p} = 0 \qquad (7.22)$$

7.6 Performance profile for the corrosion propagation phase

7.6.1 The corrosion mechanism

Once the aggressive agent front has reached the steel reinforcement, i.e. the performance indicators (Eq. 7.10) or (7.21) has decreased to 0, the steel corrosion is likely to start. As any redox process, corrosion is accompanied by an exchange of electrons producing a corrosion current. The redox process related to corrosion involves on the one hand the oxidation of iron and on the other hand the reduction of oxygen:

$$Fe \rightarrow Fe^{z+} + ze^{-} \text{ with } z=2 \text{ or } 3 \qquad (7.23)$$

$$2e^{-} + H_2O + \frac{1}{2}0_2 \rightarrow 2OH^{-} \qquad (7.24)$$

Actually, Fe^{2+} is first created and is combined with OH^- produced in (24) to form the ferrous hydroxide $Fe(OH)_2$, itself undergoing another oxidation step leading to ferric hydroxide $Fe(OH)_3$ a main component of rust in which the oxidation state of iron is 3.

The mass of steel m_s (per unit length along the rebar axis) that has reacted in the redox process can be related to the corrosion current i_{cor} (per unit length along the rebar axis) thanks to Faraday's law which reflects the stoichiometry of the oxidation equation (Eq. 7.23):

$$m_s(t) = \frac{M_s}{zF} \int_{\tau=T_{dep}}^{t} i_{cor}(\tau)\,\mathrm{d}\tau \qquad (7.25)$$

where M_s=55.85g.mol^{-1} is the molar mass of steel, z is the valency number (2 or 3) and F=96485C.mol^{-1} is the Faraday constant. The integral in (25) represents the total electric charge delivered by the oxidation process. Under a simplifying assumption of constant corrosion current, this term simply becomes $i_{cor}t$.

By identification of the number of reacted steel moles with that of generated rust moles, (Eq. 7.25) allows to derive the evolution of rust mass $m_r(t)$:

$$\frac{m_r(t)}{M_r} = \frac{m_s(t)}{M_s} \Rightarrow m_r(t) = \frac{M_r}{zF} \int_{\tau=T_{dep}}^{t} i_{cor}(\tau)\,\mathrm{d}\tau \qquad (7.26)$$

where M_r denotes the rust molar mass (89.86g.mol^{-1} for $Fe(OH)_2$ and 106.87g.mol^{-1} for $Fe(OH)_3$).

Faraday's law (Eq. 7.25) and (7.26) can be rewritten involving local surface quantities, μ_s the mass of reacted steel per rebar surface, μ_r the mass of rust product per rebar surface and j_{cor} the current density from the rebar:

$$\frac{\mu_r(t)}{M_r} = \frac{\mu_s(t)}{M_s} = \frac{1}{zF}\int_{\tau=T_{dep}}^{t} j_{cor}(\tau)\,\mathrm{d}\tau \qquad (7.27)$$

It follows that the division of (Eq. 7.27) by the steel density ρ_s=7874kg.m^{-3} provides the local loss of steel thickness:

$$e(t) = \frac{\mu_s(t)}{\rho_s} = \frac{M_s}{\rho_s zF}\int_{\tau=T_{dep}}^{t} j_{cor}(\tau)\,\mathrm{d}\tau \qquad (7.28)$$

The first geometrical model of corrosion assumes that the loss of thickness is uniform around the steel rebar, which means that the latter keeps its cylindrical shape of circular section at all times (at least in a zone of a certain extension along the steel cylinder axis).

Another model of corrosion proposed in D2.2 citing (Stewart 2009) is based on the development of a localised corrosion zone (pit configuration, see Figure 7-4). The equations corresponding to this configuration are recalled hereafter with the following notations: A_{stnom} is the initial cross-sectional area, A_{pit} is the area of the pit, P_{max} is the maximum pit depth, d_b is the initial rebar diameter.

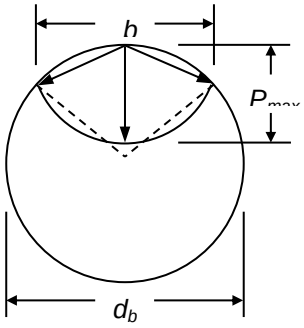

Figure 7-4 Pit configuration (Stewart 2009)

$$A_{pit}(t) = \begin{cases} \frac{1}{2}\theta_1\left(\frac{d_b}{2}\right)^2 - b\frac{d_b}{2} + \frac{1}{2}\theta_2 P_{\max}^2 & \text{if} \quad P_{\max} \le \frac{d_b}{\sqrt{2}} \\ A_{stnom} - \frac{1}{2}\theta_1\left(\frac{d_b}{2}\right)^2 - b\frac{d_b}{2} + \frac{1}{2}\theta_2 P_{\max}^2 & \text{if} \quad \frac{d_b}{\sqrt{2}} < P_{\max} \le d_b \\ A_{stnom} & \text{if} \quad P_{\max} = d_b \end{cases} \qquad (7.29)$$

with

$$A_{stnom} = \pi\left(\frac{d_b}{2}\right)^2 \quad (7.30)$$

$$b = 2P_{\max}\sqrt{1-\left(\frac{P_{\max}}{d_b}\right)^2} \quad (7.31)$$

$$\theta_1 = 2\arcsin\left(\frac{b}{d_b}\right) \quad ; \quad \theta_2 = 2\arcsin\left(\frac{b}{2P_{\max}}\right) \quad (7.32)$$

Values of P_{max} can be estimated from values of uniform corrosion P_{av}, using for example $P_{av}(t)=e(t)$ in (Eq. 7.28), and a pitting factor $R_{pit}=P_{max}/P_{av}$ with R_{pit} ranging between 4 to 8 (Gonzalez et al. 1995). Eventually, the mass of dissolved steel (per unit length along the cylinder axis) writes:

$$m_s(t) = \rho_s A_{pit}\left(P_{\max}(t)\right) = \rho_s A_{pit}\left(R_{pit}e(t)\right) \quad (7.33)$$

Although it should be difficult to determine the most relevant model to account for steel thickness loss in any situation, it is well recognized that carbonation induces more diffuse corrosion than chloride ion ingress. Consequently the model of uniform corrosion might be preferable after a carbonation phase and the one of pitting corrosion after chloride ion ingress. Nevertheless the model of uniform corrosion has also been used after an initiation phase due to chloride ion ingress (Thoft-Christensen 2000). Anyway for both cases, models rely upon the knowledge of a corrosion current which should be assessed either from in-situ measurements or provided by an empirical relationship such as (Eq. 7.43) here below.

7.6.2 Phase of crack initiation

As already stated, the first visible phenomenon induced by corrosion in the propagation phase (see Fig. 1) is concrete cracking. Indeed, corrosion products (rust) occupy a larger volume than the dissolved steel from which they have been generated. Hence the volume difference first fills a very porous zone around the rebar without mechanical effect on the solid phase. Once this zone is filled, the rust starts exerting a pressure onto the surrounding concrete, which creates orthoradial tensile stress. When the latter reaches the concrete tensile strength denoted by f_t, a crack can develop.

A simple model allowing to estimate the critical amount of produced rust leading to the initiation of crack has been proposed in (Thoft-Christensen 2000) cited by (de Cássia Silva 2004). It relies first on a simplification of the concrete zone surrounding the rebar which is the closest to the boundary and thus the most exposed to aggressive agents: this zone is replaced by a concrete thick-walled cylinder of thickness equal to the concrete cover c_p (see Figure 7-5). All the following calculations are carried out on the cross-section according to an assumption of invariance along the cylinder axis, in particular volumes of dissolved steel or produced rust are obtained by multiplying areas in the cross-section by a certain length along the cylinder axis. Moreover the framework of plain strains is adopted to account for the deformations induced by the development of pressure.

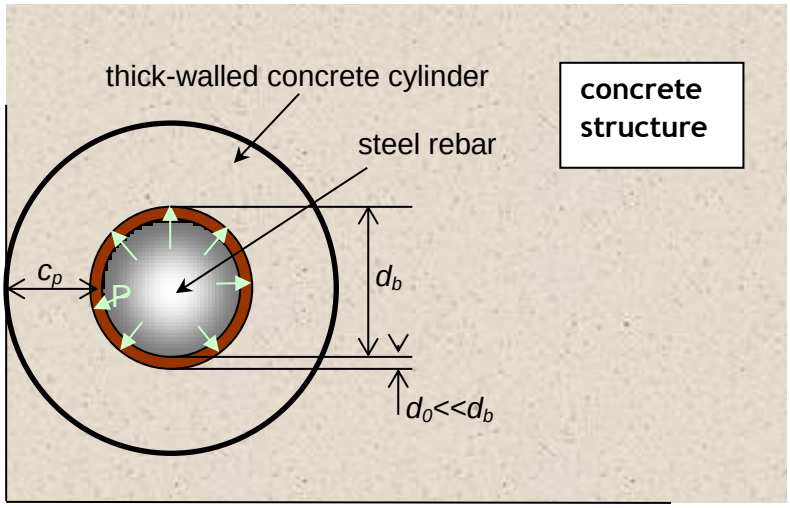

Figure 7-5 Model of concrete expansion due to corrosion (Thoft-Christensen 2000)

The increase of porosity close to the rebars, due to concrete casting, deformations at early age (shrinkage) and possibly ulterior bond weakening, is difficult to quantify. (Thoft-Christensen 2000) states that the porosity is close to one near the rebar, then decreases with the distance from the rebar to reach 0.5 at about 10-20µm. It is then suggested to model this zone by an equivalent shell of thickness d_0 of order of magnitude of several tens of micrometres and of porosity one (void zone). As this zone plays the role of a buffer postponing the initiation of cracking, a conservative decision could be to neglect it. Finally a value of d_0 between 0 and 20µm is suggested.

In the phase of pressure development, the concrete thick-walled is modelled by a linear elastic solid of Young modulus E and Poisson ratio ν. The internal radius a corresponds to the radius of the rebar $a=d_b/2$ (d_0 is neglected because of its small value) and the external radius is $b=a+c_p$ (see Figure 7-5). The relationship between the pressure induced by rust products and the radial expansion d_s of the thick-walled concrete cylinder is (Salençon 2001):

$$P = \frac{E}{a(1+\nu)\left((1-\nu)\frac{a^2+b^2}{b^2-a^2}+\nu\right)} d_s \qquad (7.34)$$

Note that (34) is slightly different from that written in (Thoft-Christensen 2000). It seems that the formula appearing in this reference corresponds to a plain stress framework.

The maximum tensile stress is reached in the orthoradial direction at the internal radius a and writes:

$$\sigma_{\theta\theta}(r=a) = \frac{a^2+b^2}{b^2-a^2} P = \frac{E}{a(1+\nu)\left((1-\nu)+\nu\frac{b^2-a^2}{a^2+b^2}\right)} d_s \qquad (7.35)$$

Radial cracking occurs when the maximum tensile stress (Eq. 7.35) reaches the tensile strength of concrete f_t, which corresponds to the following value of d_s:

$$d_s^{crack} = \frac{a(1+\nu)\left((1-\nu)+\nu\frac{b^2-a^2}{a^2+b^2}\right)}{E} f_t \qquad (7.36)$$

Neglecting the compressibility of steel and rust compared to that of concrete, the volume that can be occupied by the rust products is simply given by adding the cylindrical shell of thickness d_s^{crack} to the equivalent void zone of thickness d_0 and the volume left free by the dissolved steel. This volume balance allows to estimate the mass of rust products (per unit length along the cylinder axis) required to reach the cracking criterion:

$$\frac{m_r^{crack}}{\rho_r} = \frac{m_s^{crack}}{\rho_s} + \pi d_b (d_0 + d_s^{crack}) \qquad (7.37)$$

with the rust density ρ_r=3600kg.m^{-3} and the steel density ρ_s=7874kg.m^{-3}. If the model of uniform corrosion is adopted, (Eq. 7.37) rewrites in terms of mass per unit surface:

$$\frac{\mu_r^{crack}}{\rho_r} = \frac{\mu_s^{crack}}{\rho_s} + d_0 + d_s^{crack} \qquad (7.38)$$

Recalling the relationship (Eq. 7.26) between the dissolved steel and the produced rust masses, the following threshold values are obtained:

$$\frac{m_r^{crack}}{M_r} = \frac{m_s^{crack}}{M_s} = \frac{\pi d_b (d_0 + d_s^{crack})}{\frac{M_r}{\rho_r} - \frac{M_s}{\rho_s}} \qquad (39)$$

The performance indicator concerning concrete cracking initiation is finally built by comparing the amount of dissolved steel (Eq. 7.25) to the cracking threshold value (Eq. 7.39) or equivalently the amount of produced rust to the threshold value (Eq. 7.39) in terms of maximum rust mass :

$$P_{crack}(t) = 1 - \frac{m_s(t)}{m_s^{crack}} = 1 - \frac{m_r(t)}{m_r^{crack}} = 1 - \frac{\frac{M_r}{\rho_r} - \frac{M_s}{\rho_s}}{zF(d_0 + d_s^{crack})} \int_{\tau=T_{dep}}^{t} \frac{i_{cor}(\tau)}{\pi d_b} \mathrm{d}\tau \qquad (7.40)$$

with d_s^{crack} expressed in (Eq. 7.36).

In the case of a uniform corrosion $i_{cor}=\pi d_b j_{cor}$, (Eq. 7.40) rewrites:

$$P_{crack}(t) = 1 - \frac{\frac{M_r}{\rho_r} - \frac{M_s}{\rho_s}}{zF(d_0 + d_s^{crack})} \int_{\tau=T_{dep}}^{t} j_{cor}(\tau)\,\mathrm{d}\tau \qquad \text{(Eq. 7.41)}$$

Furthermore, if the current density is assumed constant j_{cor}, (Eq. 7.41) becomes:

$$P_{crack}(t) = 1 - \frac{\frac{M_r}{\rho_r} - \frac{M_s}{\rho_s}}{zF(d_0 + d_s^{crack})} j_{cor}\left(t - T_{dep}\right) \qquad \text{(Eq. 7.42)}$$

As mentioned in (Gonzalez 1995), typical values of 1 to 3µA.cm^{-2} are frequent in active corrosion. (Vu and Stewart 2000) proposes an empirical expression of the corrosion current density in an environment of relative humidity 75% at 20°C:

$$j_{cor}(t) = j_{cor}(1)\,0.85\,t^{-0.29} \text{ with } j_{cor}(1) = \frac{37.8(1 - w/c)^{-1.64}}{c_p} \qquad \text{(Eq. 7.43)}$$

Note that $j_{cor}(t)$ and $j_{cor}(1)$ in (Eq. 7.43) are expressed in µA.cm^{-2}.

In order to use only one model encompassing the case of constant density and (Eq. 7.43), the following generic expression can be considered:

$$j_{cor}(t) = j_{cor}(T_{dep})\left(\frac{t}{T_{dep}}\right)^{-\eta} \qquad (7.44)$$

The case of constant density is obtained for η=0 and (Eq. 7.43) for η=0.29.

The time T_{crack} required to reach the cracking criterion (in other words $P_{crack}(T_{crack})=0$) is then:

$$T_{crack} = T_{dep}\left(1 + \frac{(1-\eta)zF(d_0 + d_s^{crack})}{T_{dep}\,j_{cor}(T_{dep})\left(\frac{M_r}{\rho_r} - \frac{M_s}{\rho_s}\right)}\right)^{\frac{1}{1-\eta}} \qquad (7.45)$$

7.6.3 Phase of crack propagation

After crack initiation, unless interventions are carried out, the production of rust is assumed to continue, which causes crack opening. The following thresholds which allow the building of new performance indicators are based on limit values of the crack aperture w:

- w_{SLS}=0.3mm is considered as a limit aperture for service limit state (this limit is adopted in EUROCODE 2 for concrete bridges),
- w_{sp}=1mm corresponds to a severe situation likely to cause concrete spalling and is thus considered as a limit aperture for spalling (Val 2003).

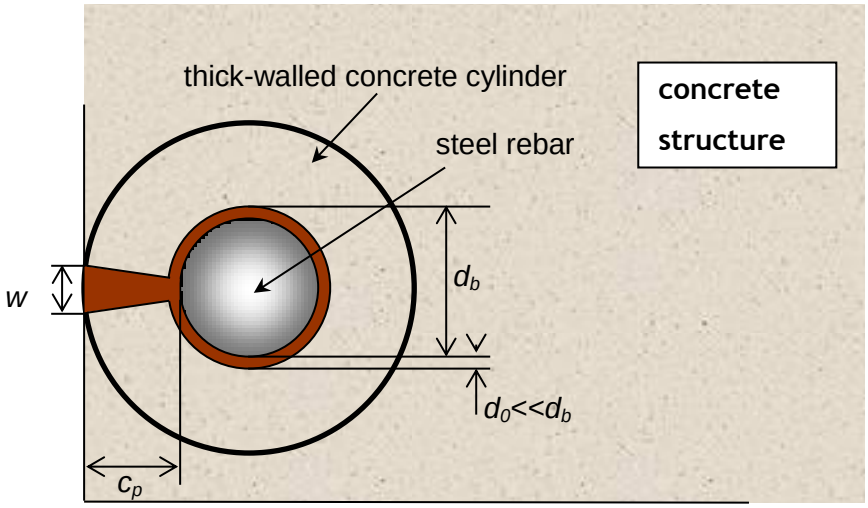

Figure 7-6 Model of crack opening (Thoft-Christensen 2000)

It remains now to find a model able to predict the crack aperture as a function of time. A simple model based on volume identity between the extra amount of rust produced since crack initiation and the space offered by the open crack is proposed in (Thoft-Christensen 2000) (see Figure 7-6). The volume balance is very similar to that leading to (Eq. 7.37) with two differences: the volume corresponding to the open crack is now considered and only mass variations from the crack initiation are accounted for (although the reasoning could equivalently be done with the whole masses starting from the corrosion initiation if the volume of the porous and the expansion zones were still included in the right hand side of the equation):

$$\frac{\Delta m_r(t)}{\rho_r} = \frac{\Delta m_s(t)}{\rho_s} + \frac{1}{2}\left(1 + \frac{d_b/2}{d_b/2 + c_p}\right) c_p w \qquad (7.46)$$

with

$$\frac{\Delta m_r(t)}{M_r} = \frac{\Delta m_s(t)}{M_s} = \frac{1}{zF} \int_{\tau=T_{crack}}^{t} i_{cor}(\tau)\,\mathrm{d}\tau \qquad (7.47)$$

Combining (7.46) and (7.47) gives the expression of *w* with respect to the corrosion current:

$$w(t) = \frac{\left(\frac{M_r}{\rho_r} - \frac{M_s}{\rho_s}\right)\frac{1}{zF}\int_{\tau=T_{crack}}^{t} i_{cor}(\tau)\,\mathrm{d}\tau}{\frac{1}{2}\left(1 + \frac{d_b/2}{d_b/2 + c_p}\right)c_p} \qquad (7.48)$$

In the model of uniform corrosion for which $i_{cor}=\square d_b j_{cor}$ and of current density (Eq. 7.44), (Eq. 7.48) becomes:

$$w(t)=\frac{\left(\frac{M_r}{\rho_r}-\frac{M_s}{\rho_s}\right)\frac{\pi d_b}{zF}\frac{j_{cor}(T_{crack})}{1-\eta}T_{crack}\left(\left(\frac{t}{T_{crack}}\right)^{1-\eta}-1\right)}{\frac{1}{2}\left(1+\frac{d_b/2}{d_b/2+c_p}\right)c_p} \quad (7.49)$$

As the two thresholds w_{SLS}=0.3mm and w_{sp}=1mm corresponding respectively to the service limit state and the concrete spalling are expressed in terms of crack aperture limits, performance indicators are naturally based on *w(t)*:

$$P_{SLS}(t)=1-\frac{w(t)}{w_{SLS}} \text{ and } P_{sp}(t)=1-\frac{w(t)}{w_{sp}} \quad (7.50)$$

The times at which the criteria are reached are therefore:

$$T_\alpha=T_{crack}\left(1+\frac{\frac{1}{2}\left(1+\frac{d_b/2}{d_b/2+c_p}\right)c_p w_\alpha}{\left(\frac{M_r}{\rho_r}-\frac{M_s}{\rho_s}\right)\frac{\pi d_b}{zF}\frac{T_{crack}\, j_{cor}(T_{crack})}{1-\eta}}\right)^{\frac{1}{1-\eta}} \text{ with } \alpha\equiv\text{"SLS" or "sp"} \quad (7.51)$$

7.6.4 Phase of structural failure

As emphasized in D2.2, the reduction of steel cross-section can lead to severe damage due to the loss of steel strength and ductility. Models showing the dependence of the latter on the corroded steel area are proposed in D2.2. Those models are linear with respect to the corroded steel area. Consequently the latter can be directly chosen as well as a conventional threshold defined as a fraction λ of the sound area (say for example λ=10% of the total cross-section area) to build a performance indicator corresponding to a risk of structural failure:

$$P_{stfail}(t)=1-\frac{\frac{m_s(t)}{\rho_s}}{\lambda\pi\left(\frac{d_b}{2}\right)^2}=1-\frac{\frac{M_s}{\rho_s zF}\int_{\tau=T_{dep}}^{t} i_{cor}(\tau)\,\mathrm{d}\tau}{\lambda\pi\left(\frac{d_b}{2}\right)^2} \quad (7.52)$$

For a uniform corrosion and the time evolution of the current density modelled by (Eq. 7.44), P_{stfail} writes:

$$P_{stfail}(t) = 1 - \frac{\frac{m_s(t)}{\rho_s}}{\lambda\pi\left(\frac{d_b}{2}\right)^2} = 1 - \frac{4M_s}{\lambda d_b \rho_s zF}\frac{j_{cor}(T_{dep})}{1-\eta}T_{dep}\left(\left(\frac{t}{T_{dep}}\right)^{1-\eta} - 1\right) \quad (7.53)$$

The time of structural failure is then given by

$$T_{stfail} = T_{dep}\left(1 + \frac{\lambda d_b \rho_s zF}{4M_s}\frac{1-\eta}{T_{dep} j_{cor}(T_{dep})}\right)^{\frac{1}{1-\eta}} \quad (7.54)$$

7.7 Example of performance profile

In order to illustrate the previously defined performance indicators, an example is developed herein and time-variant profiles are drawn. The depassivation of steel reinforcement is assumed to be reached by a carbonation mechanism. The mechanisms of concrete cracking and crack propagation (until the service limit state and the spalling criterion) are then considered, as well as structural failure. It is recalled that each criterion is reached as soon as its corresponding performance indicator becomes zero. All the parameters and hypotheses used in the performance indicators are gathered in Table 7-1. The profiles are drawn in Figure 7-7 and the resulting times of activation of the different mechanisms are reported in Table 7-2.

Table 7-1 Parameters chosen in the example of performance profiles

Parameter	Value
Carbonation phase	
w/c	0.5
g/c	5.14
ρ_c/ρ_w	2.9
ρ_g/ρ_w	2.6
c	300kg.m^{-3}
s	0
f_{C3S}	60%
ϕ^c	16%
RH	75%
$M_{Ca(OH)2}$	74g.mol^{-1}
$[CO_2]^0$	0.052mol.m^{-3}
c_p	5cm
Rust production	
ρ_s	7874kg.m^{-3}
ρ_r	3600kg.m^{-3}
M_s	55.85g.mol^{-1}
M_r	106.87g.mol-1
n	3
F	96485C.mol-1

j_{cor} constant	1µA.cm^{-2}
Cracking	
d_b	2cm
d_0	12.5µm
E	11.5GPa
ν	0.2
f_t	2.4MPa
Service limit state	
w_{SLS}	0.3mm
Spalling	
w_{sp}	1mm
Structural failure	
λ	10%

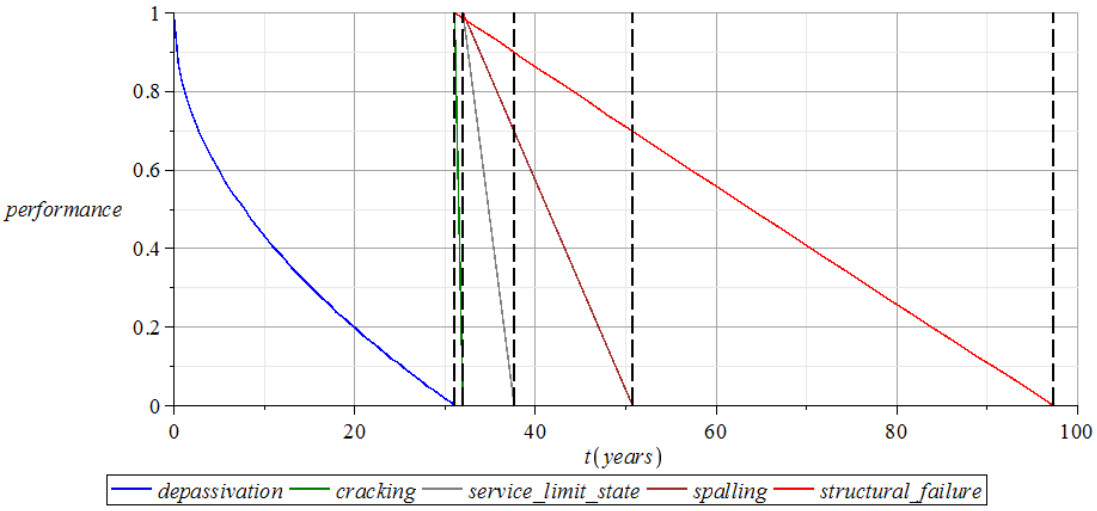

Figure 7-7 Example of performance profiles

Table 7-2 Times of activation of the degradation mechanisms

Mechanism	Value
Depassivation	31.1 years
Cracking	32.0 years
Service limit state	37.7 years
Spalling	50.9 years
Structural failure	97.4 years

The results obtained from synthetic but realistic data show that the carbonation phase may be much longer than the phase of cracking initiation, which lasts here less than one year. The following degradation mechanisms take more time to reach their limits, especially the structural failure reached after almost 100 years. As expected from their definitions, the performance indicators of the propagation phase (cracking, service limit state, spalling and structural failure) vary linearly with time whereas the performances related to the ingress of aggressive agents vary with the square root of time.

7.8 Effects of interventions

Interventions concerning concrete repairs and rehabilitations are tackled in D2.2. Several types of interventions following the observation of defects and damage are presented: structural injection of cracks, replacement of damaged corroded steel, small shallow repairs using mortar, shotcrete repairs, segmental lining repairs. They allow to repair and strengthen the structure in order to raise the performance level and/or to restore the appearance of concrete surface. Details about these interventions, their operational implementations, the conditions of application, the precautions that should be taken as well as elements influencing the repair quality are developed in D2.2. Although these interventions are precisely described, the information remains qualitative and no model which quantifies the induced increase of performance seems to be available. At least some of these interventions could be considered according to an "all or nothing" point of view. For example a complete repair of the previously damaged steel reinforcements and concrete cover should lead to a restoration of the maximum value of all performance indicators.

Electrochemical techniques should also be mentioned since they play an increasing role in repair and protection strategies. Two types of techniques can be applied (AFGC 2003).

- The first type allows restoration of the protection capacity of concrete cover against aggressive agents: re-alkalisation (against carbonation) and extraction of chloride. The principle of these treatments consists in polarizing the reinforcement nearest to the concrete surface, using an anode placed on this surface and embedded in a paste saturated with a suitably selected liquid (electrolyte). The polarization current flows from the anode towards reinforcement (cathode).
- The cathodic protection of metal reinforcement in concrete is a permanently applied treatment, which makes it possible to slow down or even stop metal corrosion. It consists in lowering the electrochemical potential of reinforcement down to a threshold value called protection potential, such that steel corrosion rate becomes negligible. The principle of cathodic protection consists in polarizing reinforcement in concrete, using an anode placed permanently on concrete surface or sometimes inside concrete cover. The polarization current, which flows from anode towards reinforcement, ranges between 2 and 50mA by square-meter of reinforcement side area.

For both techniques, either an electric power supply (impressed current technique) is placed between anode and reinforcement or the anode, made of an alloy judiciously chosen, is directly connected to reinforcement (galvanic current).

Similarly to the other intervention types, quantifying the effects of electrochemical treatments is difficult since no reliable model seems to be available. However, it is interesting to note that according to (AFGC 2003). the effects of re-alkalisation persist after 10 years, if the thickness of re-alkalized concrete around reinforcement is higher than 10 mm. Moreover, a chloride extraction is effective if chloride content in the vicinity of a reinforcement is lower than the usually allowed threshold to avoid metal corrosion. This often corresponds to an extraction of 80 to 90 % of chloride ions. It should then be emphasized that these treatments do not completely restore the concrete cover to its initial state. So putting the depassivation performance indicators to their maximum values may not correspond to a conservative decision and the best way to take the intervention into account should be to perform tests on core samples to assess the carbonation (or pH) or chloride ion profiles after the treatment in order to update the performance indicator. Nevertheless it remains to check whether the evolution of the aggressive agent front follows the same rule as before the intervention.

7.9 Conclusions for concrete-lined tunnels

Tunnel concrete linings can undergo several types of degradation (steel reinforcement corrosion, swelling mechanisms, freeze-thaw attacks) which are now rather well known at least from a qualitative point of view (see descriptions in D2.2). But modelling the evolution with time of concrete remains a difficult task because of a lack of simple time-variant performance models (i.e. not relying on heavy multi-chemo-physical numerical computations) for most of the mechanisms and a need for destructive tests for model calibration, which cannot be performed on a large number of assets. Nevertheless, the present work focused only on the deterioration induced by the corrosion of steel reinforcements after introduction of aggressive agents such as carbon dioxide or chloride ions into the concrete cover. Indeed simple models are available even though they may introduce rough approximations of more complex phenomena.

The corrosion of rebars can be decomposed into two phases: an initiation phase during which aggressive agents progressively penetrate into the concrete cover and a propagation phase starting once the aggressive agent front has reached the rebars and leading to concrete cracking and spalling until a structural failure. For each phase and each deterioration mechanism, an analytical performance indicator has been proposed and several profiles could be drawn. Still it remained difficult to quantify the effects of repair or protection on performance indicators unless the damaged rebars and concrete are completely replaced, which may allow raising the performance indicators to their initial maximum values, though partial recovery of performance may not be as simple to deal with. Indeed, it should rely on the assessment of the concrete and steel states after intervention and on the update of models if possible (through an increase of the performance profile at the time of intervention or a time shift if the material states can be related to previous known but not initial ones). Notwithstanding, this proposition may not be easily implemented.

7.10 References

AFGC (2007), “Concrete design for a given structure service life. Durability management with regard to reinforcement corrosion and alkali-silica reaction. State of the art and Guide for the implementation of a predictive performance approach based upon durability indicators.”.

AFGC (2003), “Rehabilitation of reinforced concrete damaged by corrosion.”

Bioubakhsh S. (2011), "The penetration of chloride in concrete subject to wetting and drying: measurement and modelling", Doctoral thesis, UCL (University College London)

CEN Report (2003). "Testing hardened concrete - Determination of the depth of carbonation".

CONREPNET (2001), “CONREPNET. Thematic network on performance-based remediation of reinforced concrete structures”, GTC1-2001-43067, European Commission.

de Cássia Silva R. (2004) "Contribution à l’analyse probabiliste de la performance des ponts en béton armé", PhD thesis ENPC (in French)

EN 14630 (2007). Products and systems for the protection and repair of concrete structures - Test methods - Determination of carbonation depth in hardened concrete by the phenolphthalein method.

EUROCODE 2 EN1992-2 – Design of concrete structures - Part 2: Concrete bridges - Design and detailing rules

Fagerlund G (2011), "The threshold chloride level for initiation of reinforcement corrosion in concrete. Some theoretical considerations", Lund Institute of Technology, Report TVBM-3159

Gonzalez, J.A., Andrade, C., Alonso, C., Feliu, S. (1995), “Comparison of rates of general corrosion and maximum pitting penetration on concrete embedded steel reinforcement”, Cement Conc Res, 25(2):257–264.

Hausmann D.A. (1967), "Steel corrosion in concrete: how does it occur?", Material Protection, 4(11):19-23.

Lin S. H., Taoyaun, Taiwan (1993), “Chloride diffusion in porous concrete under conditions of variable temperature” Heat & Mass Transfer (Warme- und Stoffuibertragung), 28:411-415

Otieno, M.B., Beushausen, H.S., Alexander, M.G. (2011), “Modelling corrosion propagation in reinforced concrete structures – A critical review”, Cement & Concrete Composites 33:240-5.

Papadakis V.G., Vayenas C.G., Fardis M.N. (1991a), "Fundamental modeling and experimental investigation of concrete carbonation", Am. Concr. Inst. Mater. J., 88(4):363-373

Papadakis V.G., Vayenas C.G., Fardis M.N. (1991b), "Physical and chemical characteristics affecting the durability of concrete", Am. Concr. Inst. Mater. J., 88(2):186-196

Papadakis V.G., Vayenas C.G. (1991c), "Experimental investigation and mathematical modelling of the concrete carbonation problem", Chemical Engineering Science, 46(5/6):1333-1338

RILEM Draft Recommendation, CPC-18 (1984). "Measurement of hardened concrete carbonation depth, Materials and structures", 17 (102):435-440.

Takewaka, K., and Matsumoto, S. (1988). "Quality and cover thickness of concrete based on the estimation of chloride penetration in marine environments." Concrete in Marine Environment, V. M. Malhotra, ed., SP-I09, Am. Concrete Inst. (ACI), Detroit, Mich., 381-400.

Thiery M. (2005), "Modélisation de la carbonatation atmosphérique des matériaux cimentaires. Prise en compte des effets cinétiques et des modifications microstructurales et hydriques". PhD thesis. In French.

Thoft-Christensen P. (2000), "Modelling of the Deterioration of Reinforced Concrete Structures", IFIP WG 7.5 Working Conference on Reliability and Optimization of Structural Systems, Ann Arbor, USA.

Salençon J. (2001) "Handbook of continuum mechanics. General concepts, thermoelasticity", Springer, ISBN: 3-540-41443-6

Salençon J. (2013) "Yield design", Wiley-ISTE. ISBN: 978-1-84821-540-5

Vu, K.A.T., Stewart, M.G. (2000), "Structural reliability of concrete bridges including improved chloride-induced corrosion models", Structural Safety 22:313-33.

Stewart, M.G. (2009), “Mechanical behaviour of pitting corrosion of flexural and shear reinforcement and its effect on structural reliability of corroding RC beams”, Structural Safety 31(1):19-30.

Val, D.V., Stewart, M.G. (2003), “Life-cycle cost analysis of reinforced concrete structures in marine environments”, Structural Safety 25(4):343-62.

8. Conclusion

This report focuses on the methodology developed within the MAINLINE project for constructing performance profiles for a variety of assets. It also shows specific examples of how this methodology can be implemented in producing the necessary range of profiles for the prototype LCAT tool, which is being developed as part of WP5. In order to increase its application scope, the input parameters considered cover wide ranges (e.g. different exposure environments for bridges, different types of soil for cuttings, different initial quality for track). By demonstrating the use of the LCAT tool for such a diverse range of input parameters, representative asset management scenarios across Europe can be captured and analysed. In this respect, this report, as well as the entire MAINLINE project, intends to deliver added value to different infra-owners across Europe.

Methodologies have been presented for the development of time-variant performance profiles for the following railway asset types:

- Track (plain line)
- Soil cuttings
- Tunnels with concrete lining
- Metallic bridges.

For the first two asset types, the methodologies are based on the analysis of large historical datasets pertaining to asset performance over a period of more than ten years. For the last two asset types, the methodologies are based on analytical modelling, partly based on test and field data but also relying to a considerable extent on physical understanding of the underlying deterioration mechanisms and structural behaviour. For all cases, performance profiles have been derived for a wide range of exposure and service conditions, in order to produce profiles that can be used in LCA and LCC analyses.

In general, asset performance can be managed using either condition-based or capacity-based criteria, each leading to different time-profiles. Through the selected asset types, examples have been given for both classes of criteria, with the latter (capacity-governed) being particularly relevant to the life-cycle analysis of bridges and tunnels (structural assets), whereas the former (condition-governed) are relevant to track and soil cuttings.

The results presented in this report feed into Task 5.5: Development of MAINLINE LCAT. An agreed set of performance profiles will be passed on to the main developer of the tool (SKM) in a format suitable for incorporation into Excel spreadsheets.

The sections of this report provide different levels of detail for the different asset types. Ideally the LCAT tool would require specific data about rates of deterioration in various environments and the influence that interventions have on stopping or reversing the deterioration.

In the case of Track, deterioration rates in several situations are discussed and the influences of interventions are enumerated. Some sample data are given in this document and datasets for 12 starting conditions will be developed for use in the LCAT.

The data on soil cuttings includes detailed figures for deterioration of slopes of different forms and in different initial conditions. However, the LCAT users will need to provide the necessary input with respect to the numerical effects of interventions.

Tunnels with concrete linings are assessed in respect of chemical attack on reinforcing steel by carbon dioxide and by chloride ions. An example of the rate of this deterioration rates is provided. The influence of interventions on this deterioration is difficult to evaluate in numerical terms. The presented profiles will be further developed for use in the LCAT,

although there is insufficient published information to evaluate other failure mechanisms in tunnel linings.

For metallic bridges, data is provided for the deterioration of coatings and the development of corrosion in a number of different environments and for different coating systems. Sufficient data is provided to model the deterioration of coatings and evolution of corrosion, and the influence of simple interventions, such as recoating, can be inferred from this data. The conversion of thickness lost by corrosion to bridge capacity is quantified for typical short-span half-through bridges and medium-span truss bridges. The use of the proposed normalised resistance ratios allows the assessment of a range of similar bridges. Performance profiles incorporating fatigue damage are highly specific to the exact detail geometry and the live loading characteristics throughout a bridge's life, hence they cannot be generalised for use within the current LCAT tool.

9. Appendices

APPENDIX A

The SSHI > SKMA Conversion Process: Detailed Processing Steps

The 43 individual steps applied to import and transform the SSHI data to SKMA inputs are as follows:

Step	File Name	Description
1	1. Create_Record_ID_Table_Exam.sql	This make table query combines various columns from the main cuttings examination tables for the years 2005-2012. For the purpose of this exercise we assume that a cutting is identified by the ELR and 5 chain length (5CL) that it belongs to, although in fact a cutting may extend over more than one 5CL and a given 5CL may only contain a small part of a cutting. However given that the data that we have are records of examinations rather than records of cuttings and their examination scores this is the best that we can do. The BID field provides ELR and miles and yards, and the Up_Down field provides the up/down information. The date and time information allows us to remove records that appear in more than one table (e.g. 2011 and 2012) in a subsequent query. E.g. if the most recent examination of a cutting was in 2011, then it would appear in both the 2011 and 2012 tables. The Record_ID field has been introduced as a unique identifier in the new table that is created. The MAPINFO_ID field is found to be unique within each of the individual tables and so the MAPINFO_ID field concatenated with the table year provides a unique identifier for the combined table. The Record_Type field is used to identify these records as being exam records, rather than Movement Indicator Point/Line records.
2	2.Create_Record_ID_Table_MI_Line.sql	This make table query combines various columns from the Movement Indicator Line tables for the years 2005-2012. For more information on the fields please see the comments in the query 1.Create_Record_ID_Table_Exam.
3	3.Create_Record_ID_Table_MI_Point.sql	This make table query combines various columns from the Movement Indicator Point tables for the years 2005-2012. For more information on the fields please see the comments in the query 1.Create_Record_ID_Table_Exam.
4	4. Delete_Duplicates.sql	This removes the duplicates from the tables created in steps 1-3. A record is defined to be a duplicate of another if they share the same values in the BID, Up_Down, EnteredDate and EnteredTime fields. In other words, if they describe an exam/MI recorded about the same 'cutting' at the same time. The Record_ID of the

Step	File Name	Description
		remaining record will not necessarily be from the most recent table but any table in which it appears should suffice.
5	5.Create_Records_All_Years_Exam.sql	This query combines the exam records from the various years into one table, using the record IDs selected in step 1 and step 4. Not every field appears in every year, and so the common fields have to be listed explicitly rather than using *. The data in the uncommon fields are not relevant to the current exercise.
6	6.Create_Records_All_Years_MI_Line.sql	This query combines the MI Line records from the various years into one table, using the record IDs selected in step 2 and step 4. Not every field appears in every year, and so in some cases the common fields have to be listed explicitly rather than using *. In particular the following fields appear only in the 2011 and 2012 tables: MI_Items, MI_Items_MLUP, MI_Found, MI_Repaired, NoScore, Completed. The difference between the MI_Items and MI_Observed fields is not clear. However in order that a comparison can be made with earlier exams, the MI_Observed field will be used to identify the movement indicators.
7	7.Create_Records_All_Years_MI_Point.sql	This query combines the MI Point records from the various years into one table, using the record IDs selected in step 2 and step 4. Not every field appears in every year, and so in some cases the common fields have to be listed explicitly rather than using *. In particular the following fields appear only in the 2011 and 2012 tables: MI_Items ,MI_Items_MLUP ,MI_Found ,MI_Repaired ,NoScore, Completed The difference between the MI_Items and MI_Observed fields is not clear. However in order that a comparison can be made with earlier exams, the MI_Observed field will be used to identify the movement indicators.
8	8. Create_Record_ID_Valid_SSHI_Score.sql	This query identifies the records for which we have 'valid' exam records. This is taken to mean that the information relevant to identifying an exam (BID, Up_Down, EnteredDate and EnteredTime) is not null, and also that the exam has been given / can be given a valid SSHI score. In this case it turns out that the scores occurring that aren't valid are 0 and 9.09, so these are filtered out.
9	9. Create_Record_ID_Repeat_Exams.sql	This query uses a number of derived tables to create a list of record IDs relating to cuttings that have been examined more than once (not on the same day). The first derived table OneExamPerDayV1 filters out exam dates

Step	File Name	Description
		where there has been more than one exam on that day (for a particular cutting). The second derived table CuttingsWithRepeats filters out cuttings that have only been examined once (on one day only). The third derived table OneExamPerDayV2 is the same as OneExamPerDayV1. It is joined with CuttingsWithRepeats so that the cuttings with repeats can be paired with their exam dates. This forms the fourth derived table CuttingsWithExamDates. Finally this is joined with the Record_ID_Valid_SSHI_Score table so that the CuttingsWithExamDates can be paired with their record IDs. This is put into a new table called Record_ID_Repeat_Exams.
10	10.Create_Record_ID_Exam_Ranking.sql	This query creates a table that identifies whether an exam is the 1st, 2nd, 3rd etc for a particular cutting. The Exam1, Exam2 etc. fields are constructed in order to facilitate the next query. There are enough columns for 8 exams since this is the greatest number of exams that any one cutting has.
11	11.Create_Record_ID_Exam_A_Exam_B.sql	This query takes multiple copies of the table produced by the query 10.Create_Record_ID_Exam_Ranking and produces pairs of exams, known as Exam_A and Exam_B. For example, a cutting that has been examined three times would appear twice since there are two pairs of exams, (Exam 1, Exam 2) and (Exam 2, Exam 3). Each of the select sub-queries that are unioned are used to identify if there is an (Exam 1, Exam 2) pair, (Exam 2, Exam 3) pair, and so on.
12	12.Create_Record_ID_Soil_Type_Codes.sql	This query identifies record IDs with their soil types, based on the materials given for the cutting's toe and crest. The assumption is that unless both toe and crest are of the same material the slope shall be described as a 'inter-bedded'. When one of the toe or crest materials is unknown but the other is not then the slope will be described as inter-bedded. If both are unknown then they will be described as unknown and excluded from future analysis.
13	13a. Create_Exam_A_Exam_B_ALF_Score.sql	This query returns the ALF score in the SKM algorithm for the 25,124 pairs of repeat exams. It is based on the SSHI fields Slope_Angle_Adjacent, Adjacent_Land_Drainage and Adjacent_Geomorphology. For details for the logic of the mapping between SSHI and SKMA, see the accompanying Excel file: ALF Lookup.xlsx.

Step	File Name	Description
		This query creates a table called Exam_A_Exam_B_ALF_Score and will be joined with another relating to SHF and SAF to create base value scores (ALF + SAF + SHF) in the SQL file 13c.Create_Exam_A_Exam_B_BV_Score. This table also contains information about the slope soil type.
14	13b. Create_Exam_A_Exam_B_SAF_SHF_Score.sql	This query returns the SAF and SHF scores in the SKM algorithm for the 25,124 pairs of repeat exams. It is based on the SSHI field Slope_Angle_Height. For details for the logic of the mapping between SSHI and SKMA, see the accompanying Excel file: SAF and SHF Lookup.xlsx. This query creates a table called Exam_A_Exam_B_SAF_SHF_Score which will be joined with a table relating to ALF scores to create base value scores (ALF + SAF + SHF) in the SQL file 13c.Create_Exam_A_Exam_B_BV_Score.
15	13c. Create_Exam_A_Exam_B_BV_Score.sql	This query combines the ALF, SAF and SHF scores created in queries 13a and 13b and creates the overall BV score for each pair of exams. Since this is meant to describe a constant feature of the slope then in theory it should be the same for both Exam A and Exam B. Where this is not the case, the BV score is given as 999, which excludes it from the remainder of the process. When one of Exam A or Exam B does not have a valid score, the score that is valid has been allocated in the Allocated_BV_Score field. The query creates a table called Exam_A_Exam_B_BV_Score.
16	14a.Create_Animal_Activity_Lookup.sql	This query creates a lookup that extracts the alphanumeric codes related to burrowing from the strings that are in the "Animal Activity" field in the SSHI data. The table is imported into Excel and scores assigned using the SKMA scoring system. The document is called BA Score Lookup.xlsx. The table is then reimported and used in query 14b.
17	14b.Create_Exam_A_Exam_B_BA_Score.sql	This query uses the lookup that has been created in (BA Score Lookup.xlsx) to assign scores to each record using the Animal Activity field.
18	15a.Create_Construction_Activity_Toe_Lookup.sql	This query creates a lookup that extracts the alphanumeric codes related to construction from the strings that are in the "Construction Activity Toe" field in the SSHI data.

Step	File Name	Description
		The table is imported into Excel and scores assigned using the SKMA scoring system. The document is called CA Score Lookup.xlsx. The table is then reimported and used in query 15b.
19	15b.Create_Exam_A_Exam_B_CA_Score.sql	This query uses the lookup that has been created in (CA Score Lookup.xlsx) to assign scores to each record using the Construction Activity Toe field.
20	16a.Create_Movement_Indicator_Line_Lookup.sql	This query creates a lookup that extracts the alphanumeric codes related to Movement Indicators (Line) from the strings that are in the "MI_Observed" field in the SSHI data. This is put into a table called MI_Observed_Line_Lookup.
21	16b.Create_Movement_Indicator_Point_Lookup.sql	This query creates a lookup that extracts the alphanumeric codes related to Movement Indicators (Point) from the strings that are in the "MI_Observed" field in the SSHI data. This is put into a table called MI_Observed_Point_Lookup.
22	16c.Create_MA_Features.sql	This query identifies the movement indicator numerical codes (from the MI_Observed and MI_Parameter fields) that correspond to the movement assessment features listed in SKM's algorithm. The mapping between the SSHI alphanumerics and the SKMA features is presented in the accompanying Excel document MA Score Lookup.xlsx. The query joins together the movement indicators from the Line and Point tables.
23	16d.Create_Exam_A_MA_Features.sql	This query creates a list of Exam IDs for Exam A and any movement features as listed in the SKMA. This is done firstly for Line which is then unioned with the Point equivalent. BID, Up_Down and Entered_Date are used to match MI records to their exams. This is repeated for Exam B in query 16e. They are done separately for simplicity's sake.
24	16e.Create_Exam_B_MA_Features.sql	This query creates a list of Exam IDs for Exam B and any movement features as listed in the SKMA. This is done firstly for Line which is then unioned with the Point equivalent. BID, Up_Down and Entered_Date are used to match MI records to their exams.

Step	File Name	Description
		This is repeated for Exam A in query 16d. They are done separately for simplicity's sake.
25	16f.Create_Exam_A_Exam_B_MA_Score.sql	--This query combines the Exam_A_MA_Features table and the Exam_B equivalent and assigns a the maximum --MA score, using the MA_Scores_Lookup table. It also adds in soil type and date.
26	17a.Create_Slope_Face_Condition_Lookup.sql	This query creates a lookup that extracts the alphanumeric codes related to slope face drainage condition from the strings that are in the "Slope_Face_Condition" field in the SSHI data. This is put into a table called Slope_Face_Drainage_Lookup.
27	17b.Create_Cutting_Slope_Erosion_Lookup.sql	This query creates a lookup that extracts the alphanumeric codes related to slope face drainage condition from the strings that are in the "Cutting_Slope_Erosion" field in the SSHI data. This is put into a table called Cuting_Slope_Erosion_Lookup.
28	17c.Create_SA_Features.sql	This query identifies matches the SSHI alphanumerics relating to surface water to the features described in the SKM algorithm. It makes use of the two tables created in queries 17a and 17b which relate to slope erosion and slope face condition, and also the two movement indicator tables created in queries 16a and 16b. The mapping between the SSHI alphanumerics and the SKMA features is given in the Excel document SA Score Lookup.xlsx.
29	17d.Create_Exam_A_SA_Features.sql	This query creates a list of Exam IDs for Exam A and any surface water features as listed in the SKMA. This is done firstly for the cutting slope erosion field, the slope face condition, then MI_Line and MI_Point. This is repeated for Exam B in query 17e. They are done separately for simplicity's sake.
30	17e.Create_Exam_B_SA_Features.sql	This query creates a list of Exam IDs for Exam B and any surface water features as listed in the SKMA. This is done firstly for the cutting slope erosion field, the slope face condition, then MI_Line and MI_Point. This is repeated for Exam A in query 17d. They are done separately for simplicity's sake.
31	17f.Create_Exam_A_Exam_B_SA_Score.sql	This query combines the Exam_A_SA_Features table and the Exam_B equivalent and assigns a the maximum SA score, using the SA_Scores_Lookup table. It also adds in soil type and date.

Step	File Name	Description
32	18a.Create_Tree_Cover_Lookup.sql	This query creates a lookup that extracts the alphanumeric codes related to tree cover from the strings that are in the "Tree Cover" field in the SSHI data. This is put into a table called Tree_Cover_Lookup.
33	18b.Create_Ground_Cover_Lookup.sql	This query creates a lookup that extracts the alphanumeric codes related to ground cover from the strings that are in the "Ground Cover" field in the SSHI data. This is put into a table called Ground_Cover_Lookup.
34	18c.Create_VA_Features.sql	This query identifies matches the SSHI alphanumerics relating to vegetation to the features described in the SKM algorithm. It makes use of the two tables created in queries 18a and 1bb which relate to ground cover and tree cover and also the two movement indicator tables created in queries 16a and 16b. The mapping between the SSHI alphanumerics and the SKMA features is given in the Excel document VA Score Lookup.xlsx.
35	18d.Create_Exam_A_VA_Features.sql	This query creates a list of Exam IDs for Exam A and any vegetation features as listed in the SKMA. This is done firstly for the tree cover field, then ground cover, then MI_Line and MI_Point. This is repeated for Exam B in query 18e. They are done separately for simplicity's sake.
36	18e.Create_Exam_B_VA_Features.sql	This query creates a list of Exam IDs for Exam B and any vegetation features as listed in the SKMA. This is done firstly for the tree cover field, then ground cover, then MI_Line and MI_Point. This is repeated for Exam A in query 18d. They are done separately for simplicity's sake.
37	18f.Create_Exam_A_Exam_B_VA_Score.sql	This query combines the Exam_A_VA_Features table and the Exam_B equivalent and assigns the maximum VA score, using the VA_Scores_Lookup table. It also adds in soil type and date.
38	19a.Create_Cutting_Crest_Drainage_Lookup.sql	This query creates a lookup that extracts the alphanumeric codes related to crest drainage from the strings that are in the "Cutting_Crest_Drainage" field in the SSHI data. This is put into a table called Cutting_Crest_Drainage_Lookup.
39	19b.Create_Cutting_Cess_Drainage_Lookup	This query creates a lookup that extracts the alphanumeric codes related to toe drainage from the strings that are in the

Step	File Name	Description
	.sql	"Cutting_Cess_Drainage" field in the SSHI data. This is put into a table called Cutting_Cess_Drainage_Lookup.
40	19c.Create_Exam_A_DA_Features.sql	This query identifies the drainage features for Exam A, using the DA_Mapping table created in the Excel file DA Score Lookup.
41	19d.Create_Exam_B_DA_Features.sql	This query identifies the drainage features for Exam B, using the DA_Mapping table created in the Excel file DA Score Lookup.
42	19e.Create_Exam_A_Exam_B_ALF_For_DA.sql	This query uses the previously created ALF score table to create fields related to ALF that indicate which scoring should be used in the drainage scoring.
43	19f.Create_Exam_A_Exam_B_DA_Score.sql	This query assigns scores to the drainage features identified for Exam A and Exam B.

APPENDIX B

Deterioration of Soil Cutting Score over 5 years

The tables below show the starting values of each of the six score (Input scores) and the expected values for the change in score after five years. The changes for cohesive, granular and inter-bedded soils are shown separately.

Input scores					
MA	VA	SW	DA	BA	CA
Movement Assessment	Vegetation Assessment	Surface Water Assessment	Drainage Assessment	Burrowing Assessment	Construction Activity Assessment
0.0	0.0	0.0	-1.0	0.0	0.0
1.0	0.2	1.0	0.0	1.0	1.0
1.5	0.3	1.5	0.5	2.0	2.0
2.0	0.5	2.0	1.5	-	-
2.5	1.0	2.5	-	-	-
4.0	1.5	3.0	-	-	-
5.0	-	-	-	-	-

Cohesive					
MA	VA	SW	DA	BA	CA
Movement Assessment	Vegetation Assessment	Surface Water Assessment	Drainage Assessment	Burrowing Assessment	Construction Activity Assessment
0.00	0.48	0.69	1.04	0.57	0.05
1.27	0.49	0.64	0.35	0.42	0.00
1.68	0.79	0.63	0.16	0.00	0.00
0.62	0.81	0.79	0.00		
0.22	0.03	0.22			
0.00	0.00	0.00			
0.00					

Granular					
MA	VA	SW	DA	BA	CA
Movement Assessment	Vegetation Assessment	Surface Water Assessment	Drainage Assessment	Burrowing Assessment	Construction Activity Assessment
0.00	0.32	0.27	0.94	0.49	0.05
0.45	0.27	0.55	0.16	0.39	0.03
1.15	0.57	0.62	0.23	0.00	0.00
0.13	0.30	0.32	0.00		
0.08	0.03	0.12			
0.00	0.00	0.00			
0.00					

Inter-bedded					
MA	VA	SW	DA	BA	CA
Movement Assessment	Vegetation Assessment	Surface Water Assessment	Drainage Assessment	Burrowing Assessment	Construction Activity Assessment
0.00	0.73	0.71	1.89	0.47	0.10
0.93	0.50	0.71	0.41	0.53	0.04
1.54	1.25	0.78	0.34	0.00	0.00
0.49	1.56	0.99	0.00		
0.15	0.05	0.15			
0.28	0.00	0.00			
0.00					